6
Jet properties beyond fixed order

We illustrated in Chapter 3 the use of perturbation theory to calculate 'infra-red safe' quantities such as the e^+e^- total cross section and thrust distribution. There are in addition predictions that can be made concerning some quantities that are 'infra-red sensitive', *i.e.* that have infra-red and collinear singularities in perturbation theory. Such quantities can still be handled provided the singularities can be collected into an overall factor which describes the sensitivity of the quantity to long-distance physics. The divergence of this factor corresponds to the fact that long-distance phenomena are not reliably predicted by perturbation theory. For example, quarks and gluons are free to propagate over macroscopic distances in perturbation theory, whereas in reality they are confined inside hadrons. Therefore the divergent factor should be replaced by a finite factor determined experimentally by measurements at a relatively short distance scale. Once this is done, perturbation theory can be used to predict the scale dependence of the quantity.

The best known example of a perturbative prediction of a factorizable infra-red-sensitive quantity is the phenomenon of scaling violation, discussed in Chapter 4. There we studied the parton distributions inside a hadron, probed by deep inelastic lepton scattering. Here we consider the related phenomenon for the fragmentation of a jet, produced for example in e^+e^- annihilation, into hadrons of a given type h.

6.1 Jet fragmentation

We start by defining *fragmentation functions*, which are dimensionless functions that describe single particle distributions in the final state. The total fragmentation function for hadrons of type h in e^+e^- annihilation

Downloaded from https://www.cambridge.org/core. UNIVERSIDAD AUTONOMA METROPOLITANA, on 15 Nov 2026 at 13:15:21, subject to the Cambridge Core terms of use, available at https://www.cambridge.org/core/terms. https://doi.org/10.1017/CBO9780511628788.007

at c.m. energy $\sqrt{s}$ is defined as

$$F^h(x,s) = \frac{1}{\sigma_{\rm tot}} \frac{d\sigma}{dx}(e^+e^- \to hX) \tag{6.1}$$

where $x = 2E_h/\sqrt{s} \leq 1$ is the scaled hadron energy (in practice, the approximation $x = x_p = 2p_h/\sqrt{s}$ is often used). Since each hadron of type h contributes to the fragmentation function (6.1), its integral with respect to x gives the average multiplicity of those hadrons:

$$\langle n_h(s) \rangle = \int_0^1 dx\, F^h(x,s) \,. \tag{6.2}$$

Similarly, the integral of $x\, F^h(x,s)$ gives the total scaled energy carried by hadrons of that type, which implies the sum rule

$$\sum_h \int_0^1 dx\, x\, F^h(x,s) = 2 \,. \tag{6.3}$$

The fragmentation function (6.1) can be represented as a sum of contributions from the different primary partons $i = u, d, \ldots, g$:

$$F^h(x,s) = \sum_i \int_x^1 \frac{dz}{z} C_i(s;z,\alpha_S) D_i^h(x/z,s) \,. \tag{6.4}$$

In lowest order the coefficient function C_g for gluons is zero, while for quarks $C_i = g_i(s)\delta(1-z)$ where $g_i(s)$ is the appropriate electroweak coupling. In particular, $g_i(s)$ is proportional to the charge-squared of parton i at $s \ll M_Z^2$, when weak effects can be neglected.

We cannot compute the fragmentation functions D_i^h from perturbation theory, since the production of hadrons is not a perturbative process. We might consider trying to compute functions D_i^j that would describe the fragmentation of partons of type i into partons of type j. However, they would be infinite, since the probability of emitting a collinear gluon or light quark is divergent. Nevertheless, as for the parton distribution functions $f_i(x,t)$ in deep inelastic scattering, one can show [1] that at high values of the energy-squared scale t all such divergences are factorizable, in the sense that we can write

$$D_i^j(x,t) = \sum_k \int_x^1 dz\, K_i^k(z,t,t_0)\, D_k^j(x/z,t_0) \,, \tag{6.5}$$

where the kernel function K_i^k is perturbatively calculable and at $t_0 = t$ we have $K_i^k(z,t,t) = \delta_{ik}\,\delta(1-z)$.

In the real world, hadrons are formed and fragmentation functions are not divergent. As long as the scales t and t_0 are large, we would not expect the form of Eq. (6.5) to be affected by such long-distance phenomena. Therefore we replace j by h and apply the equation to hadronic

Downloaded from https://www.cambridge.org/core. UNIVERSIDAD AUTONOMA METROPOLITANA, on 15 Nov 2026 at 13:15:21, subject to the Cambridge Core terms of use, available at https://www.cambridge.org/core/terms. https://doi.org/10.1017/CBO9780511628788.007

fragmentation functions. After measuring these functions at some scale t_0, we can use the equation to predict their form at any other scale t, as long as both t and t_0 are large enough for perturbation theory to be applicable in the calculation of the kernel K_i^k.

6.1.1 Scaling violation

The approach outlined above is very close to that adopted for the analysis of the scale dependence of parton distribution functions in Chapter 4. In a fragmentation function x represents the fraction of a parton's momentum carried by a produced hadron, whereas in a parton distribution it represents the fraction of a hadron's momentum carried by a constituent parton. In both cases, the simplest parton-model approach, represented by the independent fragmentation model (Section 5.6.1) in the case of fragmentation, would predict a scale-independent x distribution. Furthermore we obtain similar violations of this scaling behaviour when QCD corrections are taken into account.

Consider the change in a fragmentation function $D_i(x,t)$ or a parton distribution function $f_i(x,t)$ when the scale is increased from t to $t+dt$. As discussed in Section 5.2, such a change can only occur via the splitting of a parton of type i in this scale interval. Hence the fragmentation functions satisfy evolution equations like those for parton distributions:

$$t\frac{\partial}{\partial t}D_i(x,t) = \sum_j \int_x^1 \frac{dz}{z}\frac{\alpha_S}{2\pi}P_{ji}(z,\alpha_S)D_j(x/z,t)\,. \tag{6.6}$$

Notice that the splitting function is now P_{ji} rather than P_{ij} since here D_j represents the fragmentation of the final parton, whereas f_j in Eq. (5.37) represented the distribution of the initial parton. The splitting functions again have perturbative expansions of the form

$$P_{ji}(z,\alpha_S) = P_{ji}^{(0)}(z) + \frac{\alpha_S}{2\pi}P_{ji}^{(1)}(z) + \cdots \tag{6.7}$$

where the lowest-order functions $P_{ji}^{(0)}(z)$ are the same as those in deep inelastic scattering but the higher-order terms are different. The effect of splitting is, however, the same in both cases: as the scale increases, one observes a scaling violation in which the x distribution is shifted towards lower values.

As in the case of the parton distribution functions, the most common strategy for solving the evolution equations (6.6) is to take moments (Mellin transforms) with respect to x:

$$\tilde{D}(j,t) = \int_0^1 dx\; x^{j-1}\; D(x,t)\,, \tag{6.8}$$

Downloaded from https://www.cambridge.org/core. UNIVERSIDAD AUTONOMA METROPOLITANA, on 15 Nov 2026 at 13:15:21, subject to the Cambridge Core terms of use, available at https://www.cambridge.org/core/terms. https://doi.org/10.1017/CBO9780511628788.007

the inverse Mellin transformation being

$$D(x,t) = \frac{1}{2\pi i}\int_C dj\; x^{-j}\;\tilde{D}(j,t)\,, \tag{6.9}$$

where the integration contour C in the complex j plane is parallel to the imaginary axis and to the right of all singularities of the integrand. Again we can consider fragmentation function combinations which are non-singlet (in flavour space) such as $D_V = D_{q_i} - D_{\bar{q}_i}$ or $D_{q_i} - D_{q_j}$. In these combinations the mixing with the flavour singlet gluons drops out and for a fixed value of α_S the solution is simply

$$\tilde{D}_V(j,t) = \tilde{D}_V(j,t_0)\left(\frac{t}{t_0}\right)^{\gamma_{qq}(j,\alpha_S)}\,, \tag{6.10}$$

where the quantity γ_{qq} is the Mellin transform of $\alpha_S P_{qq}/2\pi$. The resulting dependence on t violates scaling rules based on naive dimensional analysis, and therefore the power γ_{qq} is called an *anomalous dimension.* For a running coupling $\alpha_S(t)$, however, the scaling violation is no longer power-behaved. Inserting the lowest-order form (2.42) for the running coupling, we find the solution

$$\tilde{D}_V(j,t) = \tilde{D}_V(j,t_0)\left(\frac{\alpha_S(t_0)}{\alpha_S(t)}\right)^{d_{qq}(j)}\,,\quad d_{qq}(j) = \frac{\gamma_{qq}^{(0)}(j)}{2\pi b}\,, \tag{6.11}$$

which varies like a power of $\ln t$.

For the singlet fragmentation function

$$D_S = \sum_i (D_{q_i} + D_{\bar{q}_i}) \tag{6.12}$$

we have mixing with the fragmentation of the gluon and the evolution equation becomes a matrix relation as in the deep inelastic scattering case:

$$t\frac{\partial}{\partial t}\begin{pmatrix}\tilde{D}_S\\ \tilde{D}_g\end{pmatrix} = \begin{pmatrix}\gamma_{qq} & 2n_f\gamma_{gq}\\ \gamma_{qg} & \gamma_{gg}\end{pmatrix}\begin{pmatrix}\tilde{D}_S\\ \tilde{D}_g\end{pmatrix}\,. \tag{6.13}$$

The anomalous dimension matrix in this equation has two real eigenvalues given by Eq. (4.140). Expressing D_S and D_g as linear combinations of the corresponding eigenvectors D_+ and D_-, we find that they evolve as superpositions of terms of the form (6.11) with γ_+ and γ_- in the place of γ_{qq}.

At small x, corresponding to $j \to 1$, the $g \to g$ anomalous dimension becomes dominant and we find $\gamma_+ \to \gamma_{gg} \to \infty$, $\gamma_- \to \gamma_{qq} \to 0$. This region requires special treatment, which will be presented in the next subsection.

As mentioned earlier, the splitting functions and anomalous dimensions for fragmentation (timelike branching) are the same as those for

Downloaded from https://www.cambridge.org/core. UNIVERSIDAD AUTONOMA METROPOLITANA, on 15 Nov 2026 at 13:15:21, subject to the Cambridge Core terms of use, available at https://www.cambridge.org/core/terms. https://doi.org/10.1017/CBO9780511628788.007

deep inelastic scattering (spacelike branching) in lowest order, as given by Eq. (4.129), but they differ in higher orders. Corresponding to Eqs. (4.107) - (4.112), in the $\overline{\rm MS}$ factorization/renormalization scheme the non-singlet timelike splitting functions (for $x \neq 1$) are [2]

$$\begin{aligned} P_{qq}^{V(1)} &= C_F^2 \left\{ \left[2\ln x \ln(1-x) + \frac{3}{2}\ln x - 2\ln^2 x \right] p_{qq}(x) \right. \\ &\quad \left. - \left(\frac{7}{2} + \frac{3}{2}x \right) \ln x + \frac{1}{2}(1+x)\ln^2 x - 5(1-x) \right\} \\ &\quad + C_F C_A \left\{ \left[\frac{1}{2}\ln^2 x + \frac{11}{6}\ln x + \frac{67}{18} - \frac{\pi^2}{6} \right] p_{qq}(x) \right. \\ &\quad \left. + (1+x)\ln x + \frac{20}{3}(1-x) \right\} \\ &\quad + C_F T_f \left\{ - \left[\frac{2}{3}\ln x + \frac{10}{9} \right] p_{qq}(x) - \frac{4}{3}(1-x) \right\} \end{aligned} \tag{6.14}$$

$$\begin{aligned} P_{q\bar{q}}^{V(1)} &= C_F \left(C_F - \frac{C_A}{2} \right) \left\{ 2p_{qq}(-x) S_2(x) \right. \\ &\quad \left. + 2(1+x)\ln x + 4(1-x) \right\} . \end{aligned} \tag{6.15}$$

Note that $P_{q\bar{q}}^{V(1)}$ is the same as in the spacelike case. The singlet functions are [3][1]

$$\begin{aligned} P_{qq}^{(1)} &= C_F^2 \left\{ -1 + x + \left(\frac{1}{2}x - \frac{3}{2} \right) \ln x + \frac{1}{2}(1+x)\ln^2 x \right. \\ &\quad \left. + \left[\frac{3}{2}\ln x - 2\ln^2 x + 2\ln x \ln(1-x) \right] p_{qq}(x) \right. \\ &\quad \left. + 2p_{qq}(-x) S_2(x) \right\} \\ &\quad + C_F C_A \left\{ \frac{14}{3}(1-x) + \left[\frac{11}{6}\ln x + \frac{1}{2}\ln^2 x + \frac{67}{18} - \frac{\pi^2}{6} \right] p_{qq}(x) \right. \\ &\quad \left. - p_{qq}(-x) S_2(x) \right\} \\ &\quad + C_F T_f \left\{ -\frac{52}{3} + \frac{28}{3}x - \left(10 + 18x + \frac{16}{3}x^2 \right) \ln x + \frac{112}{9}x^2 \right. \\ &\quad \left. - \frac{40}{9x} + 2(1+x)\ln^2 x - \left[\frac{10}{9} + \frac{2}{3}\ln x \right] p_{qq}(x) \right\} \end{aligned} \tag{6.16}$$

$$P_{qg}^{(1)} = T_f^2 \left\{ -\frac{8}{3} - \left[\frac{16}{9} + \frac{8}{3}\ln x + \frac{8}{3}\ln(1-x) \right] p_{qg}(x) \right\}$$

[1] Note that the published version of ref. [3] contains some misprints.

Downloaded from https://www.cambridge.org/core. UNIVERSIDAD AUTONOMA METROPOLITANA, on 15 Nov 2026 at 13:15:21, subject to the Cambridge Core terms of use, available at https://www.cambridge.org/core/terms. https://doi.org/10.1017/CBO9780511628788.007

$$
\begin{aligned}
&+C_F T_f \Bigg\{ -2 + 3x + (-7 + 8x) \ln x - 4 \ln(1-x) \\
&+ (1-2x) \ln^2 x + \Bigg[-2 \ln^2 (x(1-x)) - 2 \ln \left(\frac{1-x}{x} \right) \\
&+ 16 S_1(x) + 2\pi^2 - 10 \Bigg] p_{qg}(x) \Bigg\} \\
&+C_A T_f \Bigg\{ -\frac{152}{9} + \frac{166}{9} x - \frac{40}{9x} + \left(-\frac{4}{3} - \frac{76}{3} x \right) \ln x \\
&+ 4 \ln(1-x) + (2 + 8x) \ln^2 x + \Bigg[8 \ln x \ln(1-x) - \ln^2 x \\
&- \frac{4}{3} \ln x + \frac{10}{3} \ln(1-x) \\
&+ 2 \ln^2 (1-x) - 16 S_1(x) - \frac{7\pi^2}{3} + \frac{178}{9} \Bigg] p_{qg}(x) \\
&+ 2 p_{qg}(-x) S_2(x) \Bigg\}
\end{aligned} \tag{6.17}
$$

$$
\begin{aligned}
P_{gq}^{(1)} \;=\;& C_F^2 \Bigg\{ -\frac{1}{2} + \frac{9}{2} x + \left(-8 + \frac{1}{2} x \right) \ln x + 2x \ln(1-x) \\
&+ \left(1 - \frac{1}{2} x \right) \ln^2 x + \Bigg[\ln^2 (1-x) + 4 \ln x \ln(1-x) \\
&- 8 S_1(x) - \frac{4}{3} \pi^2 \Bigg] p_{gq}(x) \Bigg\} \\
&+C_F C_A \Bigg\{ \frac{62}{9} - \frac{35}{18} x - \frac{44}{9} x^2 + \left(2 + 12x + \frac{8}{3} x^2 \right) \ln x \\
&- 2x \ln(1-x) - (4 + x) \ln^2 x + p_{gq}(-x) S_2(x) \\
&+ \Bigg[-2 \ln x \ln(1-x) - 3 \ln x - \frac{3}{2} \ln^2 x - \ln^2 (1-x) \\
&+ 8 S_1(x) + \frac{7\pi^2}{6} + \frac{17}{18} \Bigg] p_{gq}(x) \Bigg\}
\end{aligned} \tag{6.18}
$$

$$
\begin{aligned}
P_{gg}^{(1)} \;=\;& C_F T_f \Bigg\{ -4 + 12x - \frac{164}{9} x^2 + \left(10 + 14x + \frac{16}{3} x^2 + \frac{16}{3x} \right) \ln x \\
&+ \frac{92}{9x} + 2(1 + x) \ln^2 x \Bigg\}
\end{aligned}
$$

Downloaded from https://www.cambridge.org/core. UNIVERSIDAD AUTONOMA METROPOLITANA, on 15 Nov 2026 at 13:15:21, subject to the Cambridge Core terms of use, available at https://www.cambridge.org/core/terms. https://doi.org/10.1017/CBO9780511628788.007

$$+C_A T_f \left\{ 2 - 2x + \frac{26}{9}\left(x^2 - \frac{1}{x}\right) - \frac{4}{3}(1+x)\ln x \right.$$
$$\left. - \left(\frac{20}{9} + \frac{8}{3}\ln x\right) p_{gg}(x) \right\}$$
$$+C_A^2 \left\{ \frac{27}{2}(1-x) + \frac{67}{9}\left(x^2 - \frac{1}{x}\right) + \left(\frac{11}{3} - \frac{25}{3}x - \frac{44}{3x}\right)\ln x \right.$$
$$-4(1+x)\ln^2 x + 2p_{gg}(-x)S_2(x) + \left[4\ln x \ln(1-x) \right.$$
$$\left. \left. -3\ln^2 x + \frac{22}{3}\ln x - \frac{\pi^2}{3} + \frac{67}{9} \right] p_{gg}(x) \right\} \qquad (6.19)$$

where $S_2(x)$ is given in Eq. (4.113) and

$$S_1(x) = \int_0^{1-x} \frac{dz}{z} \ln(1-z) \,. \qquad (6.20)$$

In terms of the dilogarithm function defined in Eq. (3.36), $S_2(x)$ is given by Eq. (4.114) and

$$S_1(x) = -\mathrm{Li}_2(1-x) = \mathrm{Li}_2(x) + \ln x \ln(1-x) - \frac{\pi^2}{6} \,. \qquad (6.21)$$

Endpoint contributions at $x = 1$ may again be evaluated using the sum rules (4.115) and (4.116). They are found to be the same as those in Eqs. (4.118)–(4.120).

The small-x limits of the splitting functions are now

$$\begin{aligned} P_{qq} &\to -\frac{\alpha_S}{2\pi}\frac{40 C_F T_f}{9x} \\ P_{qg} &\to -\frac{\alpha_S}{2\pi}\frac{40 C_A T_f}{9x} \\ P_{gq} &\to \frac{2C_F}{x} - \frac{\alpha_S}{2\pi}\frac{4 C_F C_A}{x}\ln^2 x \\ P_{gg} &\to \frac{2C_A}{x} - \frac{\alpha_S}{2\pi}\frac{4 C_A^2}{x}\ln^2 x \,. \end{aligned} \qquad (6.22)$$

Note that the higher-order terms in P_{gq} and P_{gg} are more singular as $x \to 0$ than those for deep inelastic scattering, Eq. (4.122). As a result, the resummation of enhanced terms in the fragmentation functions at small x yields a completely different behaviour from that of the small-x structure functions discussed in Section 4.6. This will be studied in detail in the following two subsections.

There are several complications in the experimental study of scaling violation in jet fragmentation functions [4]. First, the energy dependence of the electroweak couplings $g_i(s)$ that enter into Eq. (6.4) is especially

Downloaded from https://www.cambridge.org/core. UNIVERSIDAD AUTONOMA METROPOLITANA, on 15 Nov 2026 at 13:15:21, subject to the Cambridge Core terms of use, available at https://www.cambridge.org/core/terms. https://doi.org/10.1017/CBO9780511628788.007

strong in the energy region presently under study ($\sqrt{s} = 20 - 90$ GeV). In particular, the b-quark contribution more than doubles in this range. The fragmentation of the b quark into charged hadrons, including the weak decay products of the b-flavoured hadron, is expected to be substantially softer than that of the other quarks, so its increased contribution can give rise to a 'fake' scaling violation. A smaller, partially compensating effect is expected in charm fragmentation. These effects can be eliminated by extracting the b and c fragmentation functions at $\sqrt{s} = M_Z$ from tagged heavy quark events, and evolving them separately to other energies.

Secondly, one requires the gluon fragmentation function $D_g(x, s)$ in addition to those of the quarks. Although the gluon does not couple directly to the electroweak current, it contributes in higher order, and mixes with the quarks through evolution. Its fragmentation can be studied in tagged heavy-quark three-jet ($Q\bar{Q}g$) events, or via the longitudinal fragmentation function (to be discussed below).

A final complication is that power corrections to fragmentation functions, of the form $f(x)/Q^p$, are not well understood. As in the case of event shapes, Monte Carlo studies [4] suggest that hadronization can lead to $1/Q$ corrections. Therefore, possible contributions of this form should be included in the parametrization when fitting the scaling violation.

The results of an analysis of scaling violation in the charged hadron spectrum by the ALEPH collaboration [5], based on a comparison of LEP data with those from lower-energy experiments, are shown in Fig. 6.1. An overall fit in the range $22 \leq \sqrt{s} \leq 91.2$ GeV, $0.1 < x < 0.8$, incorporating full next-to-leading-order evolution and a simple parametrization of $1/Q$ power corrections, gives a good description of the data in the fitted region, as shown by the curves.[2] The fitted power corrections are small and the value obtained for $\alpha_S(M_Z^2)$ (0.126 ± 0.009) is not highly sensitive to the form assumed for them. Indeed, a leading $1/Q^2$ dependence is not ruled out, and it may be that in this case the Monte Carlo models are misleading and $1/Q$ corrections are in fact absent. An operator-product approach to fragmentation, developed in ref. [6], does indeed suggest that $1/Q$ corrections are absent.

6.1.2 *Average multiplicity*

The average number of hadrons of type h in a jet initiated by a parton i at scale t, $\langle n_h(t) \rangle_i$, is just the integral of the fragmentation function,

[2] The fitted curves do not extrapolate well into the small-x region, but a next-to-leading-order treatment would not be expected to be reliable there: see the next section.

Downloaded from https://www.cambridge.org/core. UNIVERSIDAD AUTONOMA METROPOLITANA, on 15 Nov 2026 at 13:15:21, subject to the Cambridge Core terms of use, available at https://www.cambridge.org/core/terms. https://doi.org/10.1017/CBO9780511628788.007

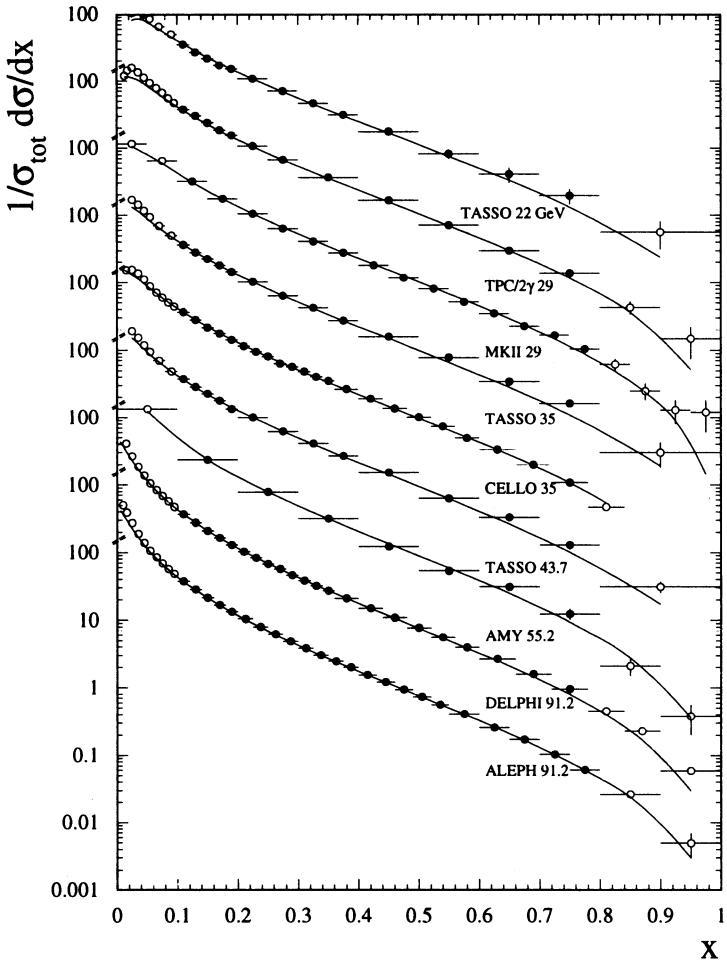


Fig. 6.1. Scaling violation in e^+e^- fragmentation functions. Figure from ref. [5].

which is the $j = 1$ moment in the notation of Eq. (6.8):

$$\langle n_h(t)\rangle_i = \int_0^1 dx\, D_i^h(x,t) = \tilde{D}_i^h(1,t)\,. \tag{6.23}$$

If we try to compute the t dependence of this quantity, we immediately encounter the problem that the lowest-order expressions for the anomalous dimensions γ_{gq} and γ_{gg} in Eq. (4.129) are divergent at $j = 1$. The reason is that for $j \leq 1$ the moments of the splitting functions in Eq. (4.94) are dominated by the region of small z, where $P_{gi}(z)$ has a divergence associated with soft gluon emission.

In fact, however, we can still solve the evolution equation for the average multiplicity provided we take into account the suppression of soft gluon

Downloaded from https://www.cambridge.org/core. UNIVERSIDAD AUTONOMA METROPOLITANA, on 15 Nov 2026 at 13:15:21, subject to the Cambridge Core terms of use, available at https://www.cambridge.org/core/terms. https://doi.org/10.1017/CBO9780511628788.007

emission due to coherence, as discussed in Chapter 5. We saw there that the leading effect of coherence is obtained simply by changing the evolution variable from virtual mass-squared to the quantity $\tilde{t} = E^2(1 - \cos\theta)$, for which the ordering condition is (5.98). Thus, after redefining t as $\tilde{t}$, Eq. (6.6) may be written in integrated form as

$$D_i(x,t) = D_i(x,t_0) + \sum_j \int_x^1 \frac{dz}{z} \int_{t_0}^{z^2 t} \frac{dt'}{t'} \frac{\alpha_S}{2\pi} P_{ji}(z,\alpha_S) D_j(x/z,t') \ , \quad (6.24)$$

or in differential form

$$t\frac{\partial}{\partial t} D_i(x,t) = \sum_j \int_x^1 \frac{dz}{z} \frac{\alpha_S}{2\pi} P_{ji}(z,\alpha_S) D_j(x/z, z^2 t) \ . \quad (6.25)$$

Notice that this differs from the conventional evolution equation (6.6) only in the z-dependent change of scale on the right-hand side. This change is not important for most values of x but we shall see that it is crucial at small x.

For simplicity, consider first the solution of Eq. (6.25) taking α_S fixed and neglecting the sum over different branchings. Then taking moments as usual we have

$$t\frac{\partial}{\partial t} \tilde{D}(j,t) = \frac{\alpha_S}{2\pi} \int_x^1 dz\, z^{j-1} P(z) \tilde{D}(j, z^2 t) \ . \quad (6.26)$$

Now if we try a solution of the form

$$D(j,t) \propto t^{\gamma(j,\alpha_S)} \quad (6.27)$$

we find that the anomalous dimension $\gamma(j,\alpha_S)$ must satisfy the implicit equation

$$\gamma(j,\alpha_S) = \frac{\alpha_S}{2\pi} \int_0^1 dz\, z^{j-1+2\gamma(j,\alpha_S)} P(z) \ . \quad (6.28)$$

When $j-1$ is not small, we may neglect the $2\gamma(j,\alpha_S)$ in the exponent of Eq. (6.28) and then we obtain the usual explicit formula for the anomalous dimension. For $j \simeq 1$, the region we are interested in, the $z \to 0$ behaviour of $P(z)$ dominates and we may as a first approximation keep only those terms that are singular at $z = 0$. The most important such term appears in the gluon-gluon splitting function: $P_{gg}(z) \to 2C_A/z$ as $z \to 0$, which implies that near $j = 1$

$$\gamma_{gg}(j,\alpha_S) = \frac{C_A \alpha_S}{\pi} \frac{1}{j - 1 + 2\gamma_{gg}(j,\alpha_S)} \quad (6.29)$$

and hence

$$\gamma_{gg}(j,\alpha_S) \ = \ \frac{1}{4}\left[\sqrt{(j-1)^2 + \frac{8C_A\alpha_S}{\pi}} - (j-1)\right]$$

Downloaded from https://www.cambridge.org/core. UNIVERSIDAD AUTONOMA METROPOLITANA, on 15 Nov 2026 at 13:15:21, subject to the Cambridge Core terms of use, available at https://www.cambridge.org/core/terms. https://doi.org/10.1017/CBO9780511628788.007

$$= \sqrt{\frac{C_A\alpha_S}{2\pi}} - \frac{1}{4}(j-1) + \frac{1}{32}\sqrt{\frac{2\pi}{C_A\alpha_S}}(j-1)^2 + \dots . \quad (6.30)$$

Thus for $j \to 1$ the gluon-gluon anomalous dimension is proportional to the square root of α_S. How can this behaviour emerge from perturbation theory, which deals only in integer powers of α_S? The answer is that at any fixed $j \neq 1$ we can expand Eq. (6.30) in a different way for sufficiently small α_S:

$$\gamma_{gg}(j,\alpha_S) = \frac{C_A\alpha_S}{\pi}\frac{1}{(j-1)} - 2\left(\frac{C_A\alpha_S}{\pi}\right)^2\frac{1}{(j-1)^3} + \dots . \quad (6.31)$$

This series displays the terms that are most singular as $j \to 1$ in each order. The first term, for example, corresponds to the fact that

$$\gamma_{gg}(j,\alpha_S) = \frac{\alpha_S}{2\pi}\gamma_{gg}^{(0)}(j) + O(\alpha_S^2) , \quad (6.32)$$

where we see from Eq. (4.129) that

$$\gamma_{gg}^{(0)}(j) = \frac{2C_A}{j-1} + \dots , \quad (6.33)$$

the dots representing terms that are not singular as $j \to 1$. The terms displayed in Eq. (6.31) just correspond to the Mellin transform of the small-x behaviour of the gluon splitting function $P_{gg}(x)$ given in Eq. (6.22). The most singular terms as $j \to 1$ ($x \to 0$) have been *resummed* in the expression (6.30), allowing the perturbation series to be analytically continued outside its circle of convergence $|\alpha_S| < (\pi/8C_A)|j-1|^2$. By definition, the behaviour outside this circle (in particular, at $j = 1$) cannot be represented by the series Eq. (6.31) any more, even though it is fully implied by it.

At sufficiently small x, the $j \to 1$ singularity of the gluon-gluon anomalous dimension dominates in all fragmentation functions, and this in turn determines the asymptotic behaviour of their first moments, *i.e.* of average multiplicities. To predict this behaviour quantitatively we need to take account of the running of α_S, which can be done in the same way as for the other moments. Writing Eq. (6.27) in the form

$$\tilde{D}(j,t) \sim \exp\left[\int^t \gamma_{gg}(j,\alpha_S)\frac{dt'}{t'}\right] , \quad (6.34)$$

we have only to replace $\gamma_{gg}(j,\alpha_S)$ in the integrand by $\gamma_{gg}(j,\alpha_S(t'))$. We then use Eq. (2.5)

$$\int^t \gamma_{gg}(j,\alpha_S(t'))\frac{dt'}{t'} = \int^{\alpha_S(t)} \frac{\gamma_{gg}(j,\alpha_S)}{\beta(\alpha_S)}\,d\alpha_S , \quad (6.35)$$

Downloaded from https://www.cambridge.org/core. UNIVERSIDAD AUTONOMA METROPOLITANA, on 15 Nov 2026 at 13:15:21, subject to the Cambridge Core terms of use, available at https://www.cambridge.org/core/terms. https://doi.org/10.1017/CBO9780511628788.007

where $\beta(\alpha_S) = -b\alpha_S^2 + \ldots$, to find

$$\tilde{D}(j,t) \sim \exp\left[\frac{1}{b}\sqrt{\frac{2C_A}{\pi\alpha_S}} - \frac{1}{4b\alpha_S}(j-1) + \frac{1}{48b}\sqrt{\frac{2\pi}{C_A\alpha_S^3}}(j-1)^2 + \ldots\right]_{\alpha_S=\alpha_S(t)} . \tag{6.36}$$

In e^+e^- annihilation the scale t (the upper limit on $E^2(1-\cos\theta)$ for any branching) is of the order of the centre-of-mass energy-squared s, and so the average multiplicity of any hadron species has the asymptotic behaviour

$$\langle n(s)\rangle = D(1,s) \propto \exp\frac{1}{b}\sqrt{\frac{6}{\pi\alpha_S(s)}} \sim \exp\sqrt{\frac{6}{\pi b}\ln\left(\frac{s}{\Lambda^2}\right)} . \tag{6.37}$$

If the next-to-leading singularities of the anomalous dimensions, *i.e.* the terms with one less power of $1/(j-1)$, are also resummed, the expression (6.37) is multiplied by a power of $\alpha_S(s)$ [7]:

$$\langle n(s)\rangle \propto \exp\left[\frac{1}{b}\sqrt{\frac{6}{\pi\alpha_S(s)}} + \left(\frac{1}{4} + \frac{5n_f}{54\pi b}\right)\ln\alpha_S(s)\right] . \tag{6.38}$$

The resulting prediction, shown by the curve in the upper part of Fig. 6.2, is in very good agreement with experiment. In this comparison there are two free parameters: the constant of proportionality in Eq. (6.38) and the scale parameter Λ_{mult} in $\alpha_S(s)$. Λ_{mult} is not necessarily equal to $\Lambda_{\overline{\text{MS}}}$, because the renormalization scheme dependence of $\langle n(s)\rangle$ only appears at next-to-next-to-leading order, and corrections to Eq. (6.38) of this order have not yet been calculated. In fact, however, the value used in Fig. 6.2, $\Lambda_{\text{mult}} = 226$ MeV, corresponding to $\alpha_S(M_Z^2) = 0.118$, is rather close to $\Lambda_{\overline{\text{MS}}}$, indicating that further higher-order corrections should be small.

We postpone discussion of the second multiplicity moment, shown in the lower part of Fig. 6.2, until Section 6.3.

6.1.3 Small-x fragmentation

The behaviour of $\tilde{D}(j,s)$ away from $j=1$ determines the form of small-x fragmentation functions via the inverse Mellin transformation (6.9). Keeping the first three terms in the Taylor expansion of the exponent, as displayed in Eq. (6.36), gives a simple Gaussian function of j which transforms into a Gaussian in the variable $\xi \equiv \ln(1/x)$:

$$xD(x,s) \propto \exp\left[-\frac{1}{2\sigma^2}(\xi-\xi_p)^2\right] , \tag{6.39}$$

Downloaded from https://www.cambridge.org/core. UNIVERSIDAD AUTONOMA METROPOLITANA, on 15 Nov 2026 at 13:15:21, subject to the Cambridge Core terms of use, available at https://www.cambridge.org/core/terms. https://doi.org/10.1017/CBO9780511628788.007

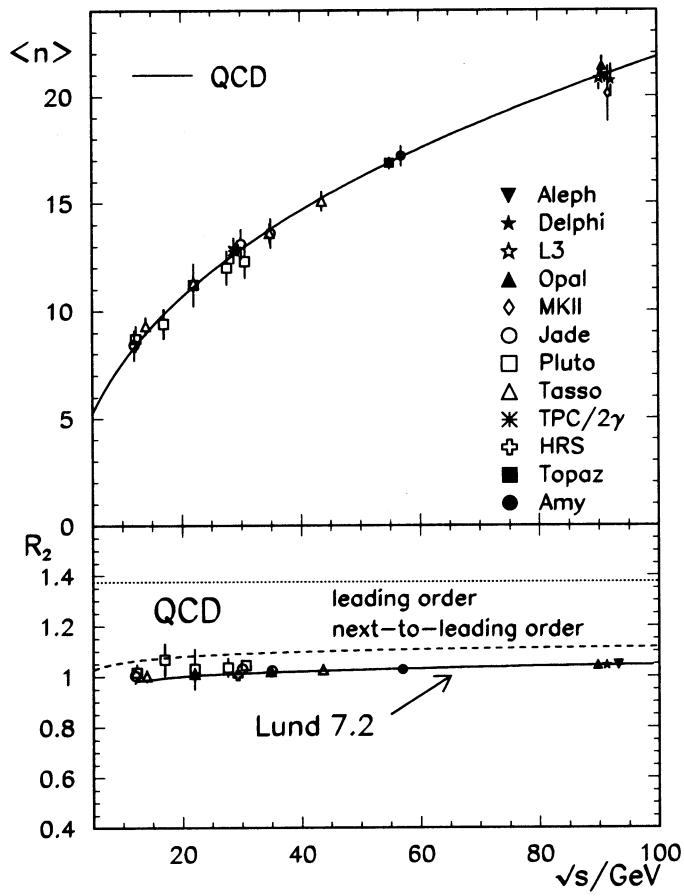


Fig. 6.2. Mean and second moment of charged hadron multiplicity in e^+e^- annihilation. Figure from ref. [8].

where the peak position is

$$\xi_p = \frac{1}{4b\alpha_S(s)} \simeq \frac{1}{4}\ln\left(\frac{s}{\Lambda^2}\right) \tag{6.40}$$

and the width of the distribution of ξ is

$$\sigma = \left(\frac{1}{24b}\sqrt{\frac{2\pi}{C_A\alpha_S^3(s)}}\right)^{\frac{1}{2}} \propto \left[\ln\left(\frac{s}{\Lambda^2}\right)\right]^{\frac{3}{4}} . \tag{6.41}$$

Again, one can compute next-to-leading corrections to these predictions. In the method of ref. [9], the corrections are included in an analytical form known as the 'modified leading logarithmic approximation' (MLLA), while in ref. [10] they are used to compute the higher moment corrections to the Gaussian form (6.39). The results of the two calculations are

Downloaded from https://www.cambridge.org/core. UNIVERSIDAD AUTONOMA METROPOLITANA, on 15 Nov 2026 at 13:15:21, subject to the Cambridge Core terms of use, available at https://www.cambridge.org/core/terms. https://doi.org/10.1017/CBO9780511628788.007

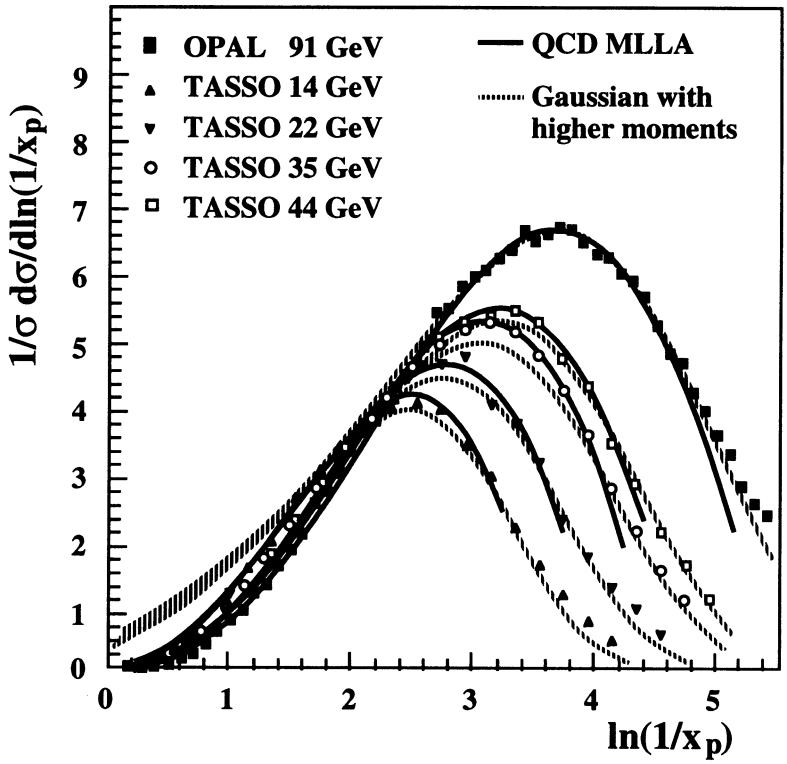


Fig. 6.3. Distribution of $\xi = \ln(1/x)$ in e^+e^- annihilation, with data from refs. [11,12]. Figure from ref. [12].

shown by the solid and broken sets of curves, respectively, in Fig. 6.3. At small x (large ξ), where they should be valid, both calculations agree well with the form and energy dependence of the measured fragmentation functions. The MLLA calculation includes some terms that become important at large x (small ξ) and therefore agrees with the data in that region as well. As in the case of the average multiplicity, the parameter Λ in Eqs. (6.40) and (6.41) should be treated as a free parameter, because the renormalization scheme sensitivity is beyond the accuracy of the present calculations. In the fits shown in Fig. 6.3, the values of Λ are 253 ± 30 MeV for the MLLA and 255 ± 26 MeV for the modified Gaussian parametrization respectively.

The predicted energy dependence (6.40) of the peak in the ξ distribution is a striking illustration of soft gluon coherence, which is the origin of the suppression of hadron production at small x. Of course, a decrease at very small x is expected on purely kinematical grounds, but this would occur at particle energies proportional to their masses, *i.e.* at $x \propto m/\sqrt{s}$

Downloaded from https://www.cambridge.org/core. UNIVERSIDAD AUTONOMA METROPOLITANA, on 15 Nov 2026 at 13:15:21, subject to the Cambridge Core terms of use, available at https://www.cambridge.org/core/terms. https://doi.org/10.1017/CBO9780511628788.007

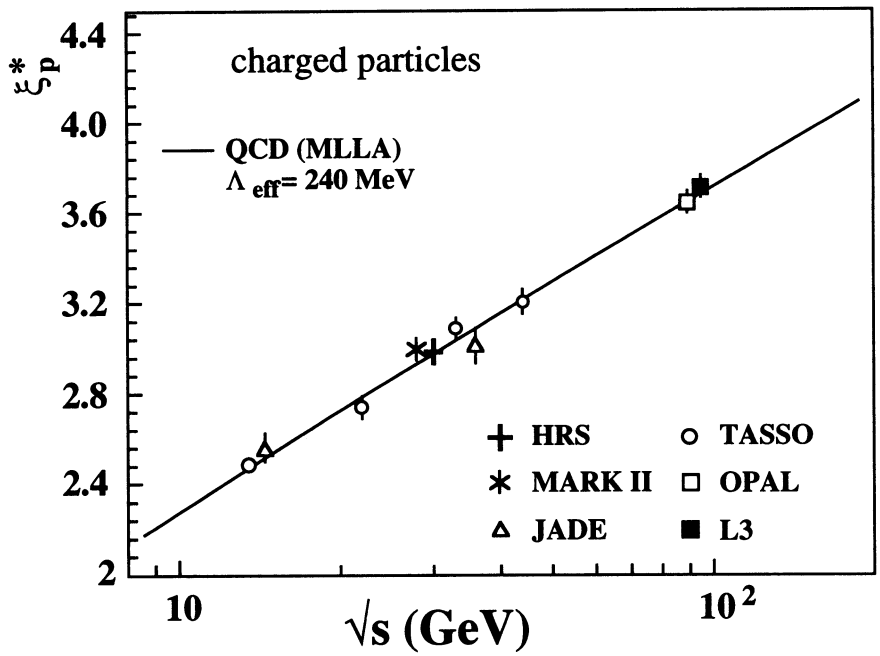


Fig. 6.4. Position of the peak in the ξ-distribution. Figure from ref. [13].

and hence $\xi \sim \frac{1}{2}\ln s$. Thus if the suppression were purely kinematic the peak position ξ_p would vary twice as rapidly with energy, which is ruled out by the data (see Fig. 6.4).

6.1.4 *Longitudinal fragmentation*

The ALEPH [5] and OPAL [14] collaborations at LEP have presented results of analyses of the longitudinal fragmentation function in e^+e^- annihilation. This is defined in terms of the joint distribution in the energy fraction x and the angle θ between the observed hadron and the incoming electron beam [4]:

$$\frac{1}{\sigma_{\rm tot}}\frac{d^2\sigma}{dx\,d\cos\theta} = \frac{3}{8}(1+\cos^2\theta)\,F_{\rm T}(x) + \frac{3}{4}\sin^2\theta\,F_{\rm L}(x) + \frac{3}{4}\cos\theta\,F_{\rm A}(x)\,, \tag{6.42}$$

where $F_{\rm T}$, $F_{\rm L}$ and $F_{\rm A}$ are respectively the transverse, longitudinal and asymmetric fragmentation functions.[3] As their names imply, $F_{\rm T}$ and $F_{\rm L}$ represent the contributions from virtual bosons polarized transversely or longitudinally with respect to the direction of motion of the hadron h.

[3] All these functions also depend on the c.m. energy $\sqrt{s}$, which we take to be fixed here.

Downloaded from https://www.cambridge.org/core. UNIVERSIDAD AUTONOMA METROPOLITANA, on 15 Nov 2026 at 13:15:21, subject to the Cambridge Core terms of use, available at https://www.cambridge.org/core/terms. https://doi.org/10.1017/CBO9780511628788.007

F_A is a parity-violating contribution which comes from the interference between the Z^0 and photon contributions. Integrating over all angles, we obtain the total fragmentation function, $F = F_T + F_L$. Each of these functions can be represented as a convolution of the parton fragmentation functions D_i with appropriate coefficient functions $C_i^{T,L,A}$ as in Eq. (6.4). The transverse and longitudinal coefficient functions are [2,15]

$$\begin{aligned} C_q^T(z) &= \delta(1-z) + O(\alpha_S) \\ C_g^T(z) &= O(\alpha_S) \\ C_q^L(z) &= C_F \frac{\alpha_S}{2\pi} + O(\alpha_S^2) \\ C_g^L(z) &= 4C_F \frac{\alpha_S}{2\pi} \left(\frac{1}{z} - 1\right) + O(\alpha_S^2) \,, \end{aligned} \tag{6.43}$$

which implies that

$$F_L(x) = C_F \frac{\alpha_S}{2\pi} \int_x^1 \frac{dz}{z} \left[F_T(z) + 4\left(\frac{z}{x} - 1\right) D_g(z)\right] + O(\alpha_S^2) \,. \tag{6.44}$$

Thus the gluon fragmentation function D_g can be extracted to leading order from measurements of F_T and F_L.

Fig. 6.5 shows the OPAL data [14] on the transverse and longitudinal fragmentation functions for charged particles. Note from Eq. (6.44) that F_L is $O(\alpha_S)$ relative to F_T; it also falls more steeply with x. Therefore even with LEP statistics the errors are large for $x > 0.3$. However, one still obtains useful information on the gluon fragmentation function over the full range of x, as shown in Fig. 6.6. Because the relation (6.44) is known only to leading order, there is an ambiguity about the energy scale at which D_g is measured. Since the gluon contribution comes from three-jet events, one might expect the appropriate scale to be about one third of the centre-of-mass energy. Comparisons with JETSET Monte Carlo predictions at scales straddling this value are shown. In Section 6.4 we shall discuss data on gluon jet fragmentation obtained more directly from three-jet events.

Similar results on the longitudinal fragmentation function have been obtained by the ALEPH collaboration [5], who include this information as a constraint on the gluon fragmentation function in their fit to scaling violation shown in Fig. 6.1.

Summed over all particle types, the total fragmentation function satisfies the energy sum rule (6.3), which we may write as

$$\frac{1}{2} \int_0^1 dx\, xF(x) = 1 \,. \tag{6.45}$$

Downloaded from https://www.cambridge.org/core. UNIVERSIDAD AUTONOMA METROPOLITANA, on 15 Nov 2026 at 13:15:21, subject to the Cambridge Core terms of use, available at https://www.cambridge.org/core/terms. https://doi.org/10.1017/CBO9780511628788.007

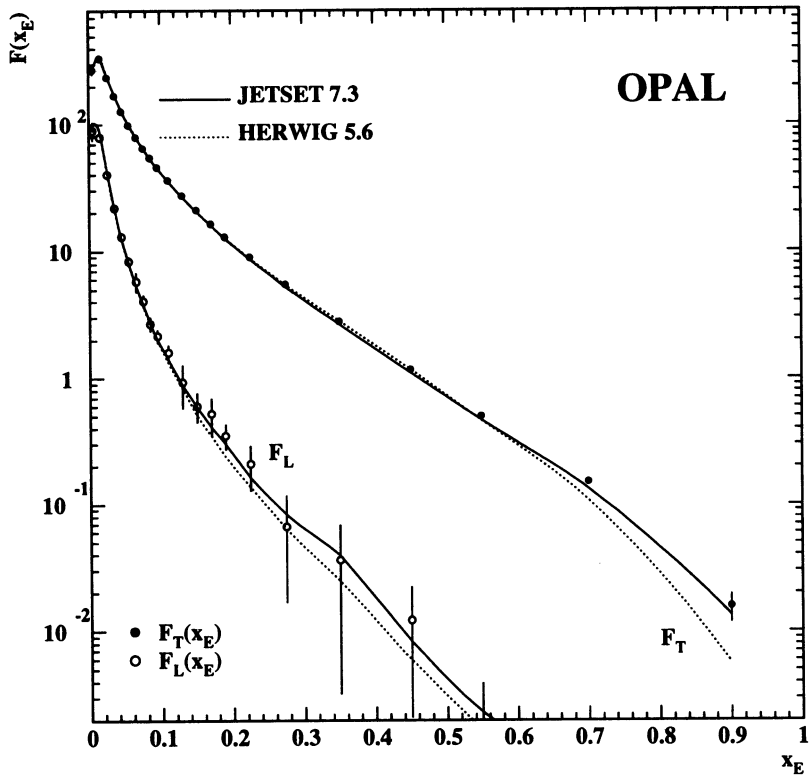


Fig. 6.5. Transverse and longitudinal fragmentation functions in $Z^0 \to$ hadrons. Figure from ref. [14].

Similarly the integrals

$$\frac{1}{2}\int_0^1 dx\, x F_{\mathrm{T,L}}(x) \equiv \frac{\sigma_{\mathrm{T,L}}}{\sigma_{\mathrm{tot}}} \tag{6.46}$$

give the transverse and longitudinal fractions of the total cross section. The perturbative prediction is [16]

$$\begin{aligned} \frac{\sigma_{\mathrm{L}}}{\sigma_{\mathrm{tot}}} &= \frac{\alpha_S}{\pi} + \left(\frac{601}{40} - \frac{6}{5}\zeta(3) - \frac{37}{36}n_f\right)\left(\frac{\alpha_S}{\pi}\right)^2 + O(\alpha_S^3) \\ &\simeq \frac{\alpha_S}{\pi} + (13.583 - 1.028 n_f)\left(\frac{\alpha_S}{\pi}\right)^2 \end{aligned} \tag{6.47}$$

where the ζ function is given in Eq. (3.19). Comparing with Eq. (3.17), we see that the whole of the $O(\alpha_S)$ correction to σ_{tot} comes from the longitudinal part, while the $O(\alpha_S^2)$ correction receives both longitudinal and transverse contributions.

The OPAL data point for $\sigma_{\mathrm{L}}/\sigma_{\mathrm{tot}}$ is shown, together with the per-

Downloaded from https://www.cambridge.org/core. UNIVERSIDAD AUTONOMA METROPOLITANA, on 15 Nov 2026 at 13:15:21, subject to the Cambridge Core terms of use, available at https://www.cambridge.org/core/terms. https://doi.org/10.1017/CBO9780511628788.007

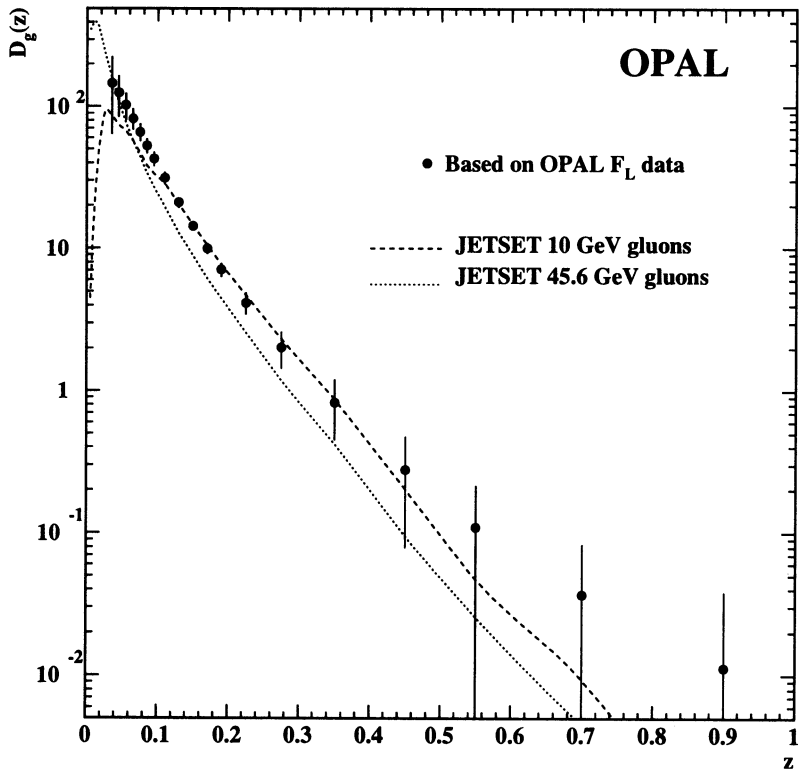


Fig. 6.6. Gluon fragmentation function extracted from $F_{T,L}$. Figure from ref. [14].

turbative predictions, in Fig. 6.7. The data lie somewhat above the next-to-leading-order prediction (dashed), which suggests that higher-order and/or non-perturbative corrections are significant. An estimate of the latter is provided by the difference between the JETSET Monte Carlo hadron-level prediction (dot-dashed) and the perturbative result. This difference shows a clear $1/Q$ behaviour, with a coefficient of about 1 GeV, illustrating once again the characteristic energy dependence of hadronization effects.

In fact, using the simple 'tube' model of hadronization discussed in Section 5.6, the correction to the longitudinal cross is found to be

$$\left\langle \frac{\delta\sigma_L}{\sigma_{tot}} \right\rangle_{had} = \frac{\pi\lambda}{2Q} \simeq \frac{0.8\ \text{GeV}}{Q}\ , \tag{6.48}$$

Adding this to the next-to-leading-order prediction gives the solid curve in Fig. 6.7, which agrees well with the JETSET prediction. The correction arises from mixing between the transverse and longitudinal angular dependences in Eq. (6.42) due to hadronization. The transverse cross

Downloaded from https://www.cambridge.org/core. UNIVERSIDAD AUTONOMA METROPOLITANA, on 15 Nov 2026 at 13:15:21, subject to the Cambridge Core terms of use, available at https://www.cambridge.org/core/terms. https://doi.org/10.1017/CBO9780511628788.007

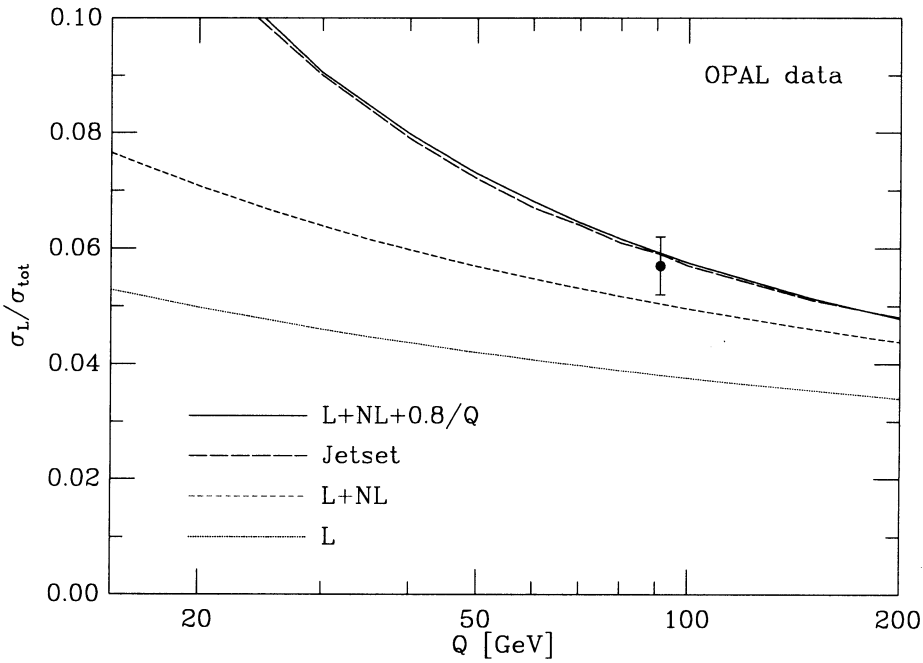


Fig. 6.7. Longitudinal fraction of the e^+e^- hadronic cross section.

section receives an equal and opposite correction, and so there is no $1/Q$ term in the total cross section.

6.1.5 *Fragmentation in deep inelastic scattering*

Jet physics in *ep* collisions promises to be a rich field of study for the new HERA collider at DESY. One can, for example, compare the properties of jets in e^+e^- and *ep* collisions, which is a good test of the factorizability of jet fragmentation functions discussed above.

The most direct comparison is between one hemisphere of an e^+e^- event, defined with respect to the thrust axis, and the 'current jet hemisphere' of deep inelastic scattering in the Breit frame [17,18]. The Breit frame is the one in which the momentum transfer from the lepton, q^μ, has only a z-component: $q^\mu = (0,0,0,Q)$. In the parton model, in this frame the struck quark enters from the right with z-momentum $p_z = -\frac{1}{2}Q$ and sees the exchanged virtual boson as a 'brick wall', from which it simply rebounds with $p_z = +\frac{1}{2}Q$. Thus the right-hand hemisphere of the final state should look like one hemisphere of an e^+e^- annihilation event at $E_{cm} = Q$. The left-hand ('beam jet') hemisphere, on the other hand, is different from e^+e^- because it contains the proton remnant, moving with momentum $p_z = -(1-x)Q/2x$ in this frame.

Downloaded from https://www.cambridge.org/core. UNIVERSIDAD AUTONOMA METROPOLITANA, on 15 Nov 2026 at 13:15:21, subject to the Cambridge Core terms of use, available at https://www.cambridge.org/core/terms. https://doi.org/10.1017/CBO9780511628788.007

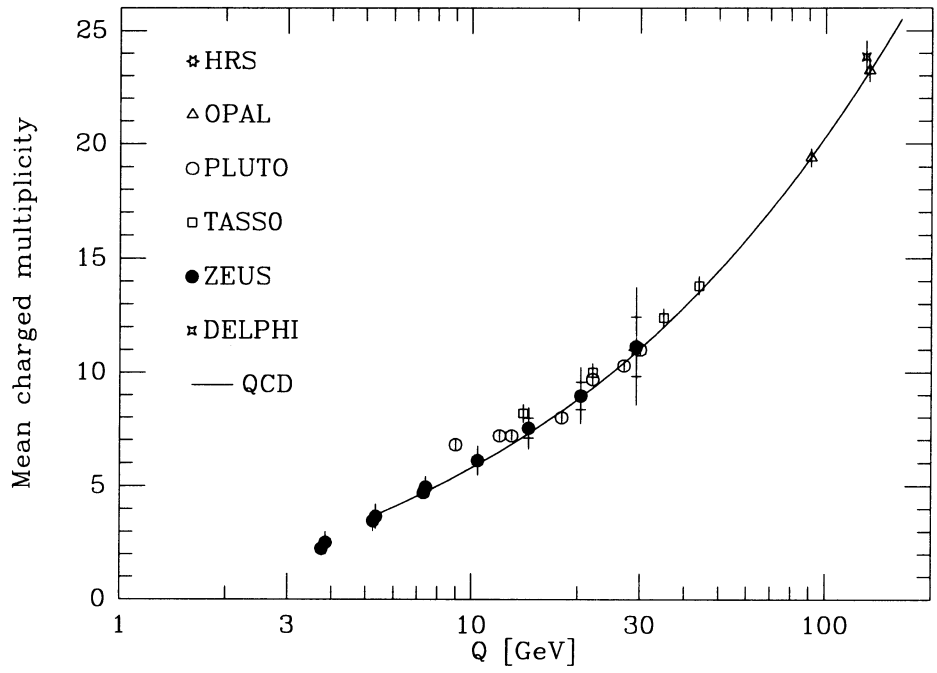


Fig. 6.8. Mean charged multiplicity in e^+e^- and ep current jet fragmentation. Adapted from ref. [19].

Fig. 6.8 shows the results of such a comparison by the ZEUS collaboration [19], in this case comparing twice the charged multiplicity in the Breit frame current hemisphere with that observed in e^+e^- annihilation (corrected for K_S and Λ^0 decays and therefore differing slightly from Fig. 6.2). The e^+e^- results are shown by the open symbols. We see that the e^+e^- and ep data are consistent. On a more detailed level, one would expect small differences, due to the different mixtures of quark flavours and higher-order corrections in the two processes. The curve shows Eq. (6.38), this time with scale parameter $\Lambda_{\text{mult}} = 1$ GeV, corresponding to the slightly more rapid increase in the ep data at low scales.

A more elaborate comparison is shown in Fig. 6.9. Here the position of the peak in the distribution of $\ln(1/x_p)$, where $x_p = 2p/Q$ in the Breit frame, is compared with that found in e^+e^- annihilation (Fig. 6.4). We see again that the HERA data exhibit the same Q-dependence as the e^+e^- data, in remarkable agreement with the theoretical predictions.

Downloaded from https://www.cambridge.org/core. UNIVERSIDAD AUTONOMA METROPOLITANA, on 15 Nov 2026 at 13:15:21, subject to the Cambridge Core terms of use, available at https://www.cambridge.org/core/terms. https://doi.org/10.1017/CBO9780511628788.007

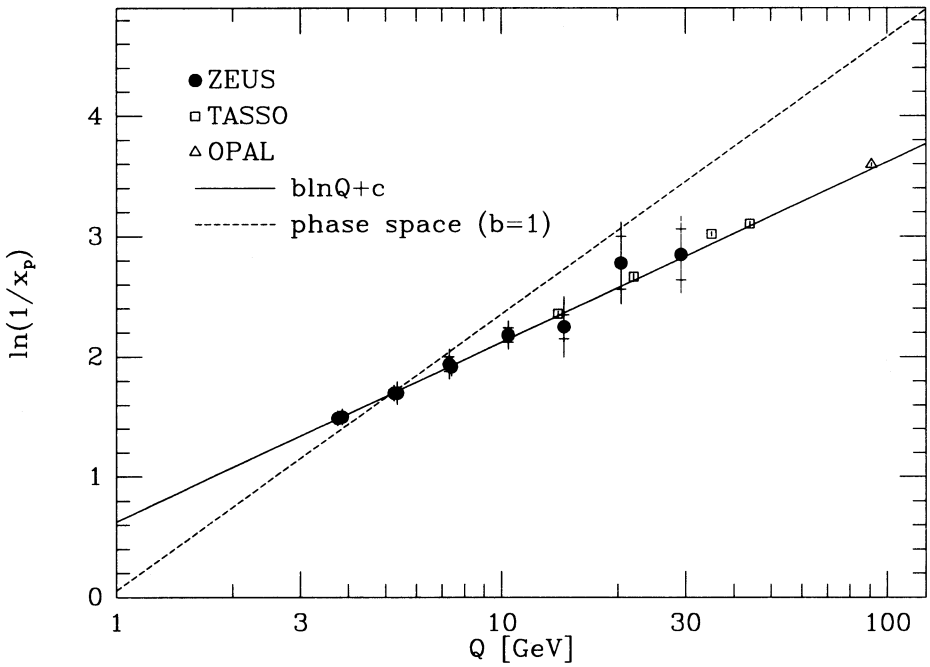


Fig. 6.9. Position of the peak in $\ln(1/x_p)$ in e^+e^- and ep current jet fragmentation. Adapted from ref. [19].

6.2 Generating function method

A useful calculational technique based on the parton branching formalism involves the use of *generating functions* or, more powerfully, *generating functionals* [9,18]. We concentrate here on the former, which are mathematically simpler. Let $P_p(n)$ represent the probability of finding n objects of a particular type in the final state of a given process p, where for example the objects could be charged hadrons and the process could be e^+e^- annihilation at a given centre-of-mass energy. Alternatively, the objects could be jets, defined by a given jet algorithm with a certain resolution $y_{\rm cut}$, see Section 3.3. The corresponding generating function is defined as

$$\phi_p(u) = \sum_{n=0}^{\infty} u^n \, P_p(n) \; . \tag{6.49}$$

We can recover the probability distribution $P_p(n)$ itself by successive differentiation at $u = 0$:

$$P_p(n) = \frac{1}{n!} \left. \frac{d^n \phi_p}{du^n} \right|_{u=0} \; . \tag{6.50}$$

Downloaded from https://www.cambridge.org/core. UNIVERSIDAD AUTONOMA METROPOLITANA, on 15 Nov 2026 at 13:15:21, subject to the Cambridge Core terms of use, available at https://www.cambridge.org/core/terms. https://doi.org/10.1017/CBO9780511628788.007

On the other hand the *binomial moments* of the distribution are obtained by differentiating at $u = 1$

$$\begin{aligned} \langle n \rangle_p &= \sum_{n=0}^{\infty} n\, P_p(n) = \left. \frac{d\phi_p}{du} \right|_{u=1} \\ \langle n(n-1)\ldots(n-k+1) \rangle_p &= \left. \frac{d^k \phi_p}{du^k} \right|_{u=1} . \end{aligned} \tag{6.51}$$

Consider specifically the case of e^+e^- annihilation. To leading order the final state is quark-antiquark and therefore the generating function is simply

$$\phi_{e^+e^-}(u) = \phi_q(u)\phi_{\bar{q}}(u) \tag{6.52}$$

where ϕ_q ($\phi_{\bar{q}}$) represents the generating function for the fragmentation of a quark (antiquark) into objects of the required type. In general there should be a sum over flavours on the right-hand side, with appropriate relative probabilities, but we shall assume flavour independence, which is a reasonable first approximation when the detected objects are charged particles or jets. In these cases the objects also form a charge-conjugation invariant set, and so $\phi_q = \phi_{\bar{q}}$. Then Eq. (6.52) becomes simply

$$\phi_{e^+e^-}(u) = [\phi_q(u)]^2 . \tag{6.53}$$

Now we derive an equation for ϕ_q, the generating function for quark fragmentation. This will depend on the scale of the hard process in which the jet is produced, which in e^+e^- annihilation is the centre-of-mass energy squared, s. As discussed in Section 5.5, to take account of coherence in jet evolution we use the scale variable $\tilde{t}$ defined by Eqs. (5.93) and (5.97), which we denote in what follows by t. Thus we write Eq. (6.53) as

$$\phi_{e^+e^-}(u, s) = [\phi_q(u, t)]^2_{t=s} . \tag{6.54}$$

The scale dependence of the generating function may be found using the parton branching formalism of Chapter 5. When a parton of type a branches into b and c, the generating function ϕ_a is replaced by $\phi_b\phi_c$. Following the steps that led to Eq. (5.49) for the parton distribution, and taking coherence into account according to Eqs. (5.98) and (5.100), we obtain

$$\begin{aligned} \phi_q(u,t) &= \phi_q(u,t_0)\Delta_q(t) + \int_{t_0}^{t} \frac{dt'}{t'} \frac{\Delta_q(t)}{\Delta_q(t')} \int dz \frac{\alpha_S(z^2(1-z)^2 t')}{2\pi} \\ &\quad \times \hat{P}_{qq}(z)\phi_q(u, z^2 t')\phi_g(u, (1-z)^2 t') . \end{aligned} \tag{6.55}$$

This equation is valid in the next-to-leading logarithmic approximation, that is, it takes account of the double logarithmic singularities generated by collinear soft gluon emission to all orders, and also the terms with

Downloaded from https://www.cambridge.org/core. UNIVERSIDAD AUTONOMA METROPOLITANA, on 15 Nov 2026 at 13:15:21, subject to the Cambridge Core terms of use, available at https://www.cambridge.org/core/terms. https://doi.org/10.1017/CBO9780511628788.007

one less logarithm due to emission that is collinear but not soft. In this approximation we can simplify the integrand considerably. The $q \to q$ splitting function is

$$\hat{P}_{qq}(z) = C_F \frac{1+z^2}{1-z} = C_F \left(\frac{2}{1-z} - 1 - z \right) \simeq C_F \left(\frac{2}{1-z} - \frac{3}{2} \right) , \quad (6.56)$$

where in the last expression we have replaced the non-singular part by its average with respect to z, since all the other terms in the integrand depend on z only logarithmically. For the same reason we may replace z by 1 in all the argument factors except for $(1-z)$ in the singular part. Writing $(1-z)^2 t' = t''$, Eq. (6.55) becomes

$$\begin{aligned} \phi_q(u,t) &= \phi_q(u,t_0)\Delta_q(t) + \frac{C_F}{2\pi} \int_{t_0}^{t} \frac{dt'}{t'} \frac{\Delta_q(t)}{\Delta_q(t')} \phi_q(u,t') \\ &\quad \times \left[\int_{t_0}^{t'} \frac{dt''}{t''} \alpha_S(t'') \phi_q(u,t'') - \frac{3}{4} \alpha_S(t') \phi_q(u,t') \right] , \quad (6.57) \end{aligned}$$

which has the solution

$$\phi_q(u,t) = \phi_q(u,t_0)\Delta_q(t) \exp \left[\int_{t_0}^{t} dt' \, \Gamma_q(t,t') \phi_g(u,t') \right] \quad (6.58)$$

where

$$\Gamma_q(t,t') = \frac{C_F}{2\pi} \frac{\alpha_S(t')}{t'} \left(\ln \frac{t}{t'} - \frac{3}{2} \right) . \quad (6.59)$$

Note that the Sudakov form factor (5.101) may be written in terms of the branching function (6.59) as

$$\Delta_q(t) = \exp \left[- \int_{t_0}^{t} dt' \, \Gamma_q(t,t') \right] . \quad (6.60)$$

Thus Eq. (6.58) satisfies the unitarity constraint $\phi_q(1,t) = \phi_g(1,t) = 1$, which follows from the definition (6.49).

The solution (6.58) is expressed in terms of the gluon jet generating function ϕ_g, which satisfies a branching equation analogous to (6.55). Making the same next-to-leading logarithmic approximations that led to Eq. (6.57), we obtain

$$\begin{aligned} \phi_g(u,t) &= \phi_g(u,t_0)\Delta_g(t) + \int_{t_0}^{t} \frac{dt'}{t'} \frac{\Delta_q(t)}{\Delta_q(t')} \Big\{ \phi_q(u,t') \\ &\quad \times \frac{C_A}{2\pi} \left[\int_{t_0}^{t'} \frac{dt''}{t''} \alpha_S(t'') \phi_g(u,t'') - \frac{11}{6} \alpha_S(t') \phi_g(u,t') \right] \\ &\quad + \frac{n_f}{6\pi} \alpha_S(t') [\phi_q(u,t')]^2 \Big\} , \quad (6.61) \end{aligned}$$

Downloaded from https://www.cambridge.org/core. UNIVERSIDAD AUTONOMA METROPOLITANA, on 15 Nov 2026 at 13:15:21, subject to the Cambridge Core terms of use, available at https://www.cambridge.org/core/terms. https://doi.org/10.1017/CBO9780511628788.007

where the last term on the right-hand side comes from the splitting $g \to q\bar{q}$. Introducing the functions

$$\begin{aligned} \Gamma_g(t,t') &= \frac{C_A}{2\pi}\frac{\alpha_S(t')}{t'}\left(\ln\frac{t}{t'} - \frac{11}{6}\right) \\ \Gamma_f(t') &= \frac{n_f}{6\pi}\frac{\alpha_S(t')}{t'}\,, \end{aligned} \tag{6.62}$$

we may write this in a form similar to Eq. (6.58):

$$\begin{aligned} \phi_g(u,t) &= \phi_g(u,t_0)\Delta_g(t)\exp\left[\int_{t_0}^{t} dt'\{\Gamma_g(t,t')\phi_g(u,t') \right. \\ &\qquad \left. + \Gamma_f(t')[\phi_q(u,t')]^2/\phi_g(u,t')\}\right] \end{aligned} \tag{6.63}$$

where

$$\Delta_g(t) = \exp\left[-\int_{t_0}^{t} dt'\{\Gamma_g(t,t') + \Gamma_f(t')\}\right]\,. \tag{6.64}$$

In the following sections we shall use these results to calculate properties of the multiplicity distributions of hadrons and sub-jets within jets.

6.3 Multiplicity distributions

In principle we can compute the energy scale dependence of the cross section for any fixed multiplicity n from the generating function equations (6.58) and (6.63). Consider, for example, the probability of producing no objects of the prescribed type (for example, no charged particles, only neutrals) in e^+e^- annihilation at c.m. energy $\sqrt{s}$. This is given by

$$\begin{aligned} P_{e^+e^-}(0,s) &= \phi_{e^+e^-}(0,s) = [\phi_q(0,s)]^2 \\ &= P_{e^+e^-}(0,t_0)[\Delta_q(s)]^2\exp\left[2\int_{t_0}^{s} dt\,\Gamma_q(s,t)\phi_g(0,t)\right]\,, \end{aligned} \tag{6.65}$$

where $\phi_g(0,t)$ is to be obtained by solving the implicit equation (6.63). We can see that it must behave roughly like $\Delta_g(t)$, which vanishes faster than any inverse power at large t. Therefore the exponent in Eq. (6.65) is asymptotically negligible and we find at high energy

$$P_{e^+e^-}(0,s) \sim P_{e^+e^-}(0,t_0)[\Delta_q(s)]^2 \tag{6.66}$$

which again vanishes faster than any power of s. In general the cross section for any fixed multiplicity may rise at low energy but must eventually become dominated by the Sudakov factor and decrease rapidly.

Another application of the generating function method is the calculation of multiplicity moments according to Eq. (6.51). For brevity, we

Downloaded from https://www.cambridge.org/core. UNIVERSIDAD AUTONOMA METROPOLITANA, on 15 Nov 2026 at 13:15:21, subject to the Cambridge Core terms of use, available at https://www.cambridge.org/core/terms. https://doi.org/10.1017/CBO9780511628788.007

introduce the following notation for the mean and first binomial moment in process p:

$$\begin{aligned} \langle n \rangle_p &\equiv N_p \\ \langle n(n-1) \rangle_p &\equiv M_p \,. \end{aligned} \tag{6.67}$$

Eq. (6.53) is valid to next-to-leading logarithmic accuracy, and so to this precision the e^+e^- moments are related to those of a quark jet as follows:

$$\begin{aligned} N_{e^+e^-} &= 2N_q \\ M_{e^+e^-} &= 2(M_q + N_q^2) \,. \end{aligned} \tag{6.68}$$

We check first that the average multiplicity is consistent with that obtained in Section 6.1.2. From Eqs. (6.58) and (6.63) we obtain the coupled integral equations

$$\begin{aligned} N_q(t) &= N_q(t_0) + \int_{t_0}^{t} dt' \, \Gamma_q(t,t') N_g(t') \\ N_g(t) &= N_g(t_0) + \int_{t_0}^{t} dt' \Big\{ \Gamma_g(t,t') N_g(t') \\ &\quad + \Gamma_f(t') [2N_q(t') - N_g(t')] \Big\} \,. \end{aligned} \tag{6.69}$$

By successive differentiation with respect to t we find

$$\begin{aligned} t\frac{d}{dt}\left(t\frac{dN_q}{dt}\right) &= \frac{C_F}{2\pi}\alpha_S(t)\left(N_g - \frac{3}{2}t\frac{dN_g}{dt}\right) \\ t\frac{d}{dt}\left(t\frac{dN_g}{dt}\right) &= \frac{C_A}{2\pi}\alpha_S(t)\left(N_g - \frac{11}{6}t\frac{dN_g}{dt}\right) \\ &\quad + \frac{n_f}{6\pi}\alpha_S(t)\, t\frac{d}{dt}(2N_q - N_g) \,. \end{aligned} \tag{6.70}$$

The asymptotic behaviour is dominated by the first term on the right-hand side in each of these equations, which gives

$$N_q(t) \sim \frac{C_F}{C_A} N_g(t) \propto \exp \frac{1}{b}\sqrt{\frac{2C_A}{\pi\alpha_S(t)}} \,, \tag{6.71}$$

in agreement with Eq. (6.37).

Now we turn to the calculation of the second moment. By differentiating Eqs. (6.58) and (6.63) twice at $u = 1$ we obtain

$$\begin{aligned} M_q(t) &= M_q(t_0) - [N_q(t_0)]^2 + [N_q(t)]^2 + \int_{t_0}^{t} dt' \, \Gamma_q(t,t') M_g(t') \\ M_g(t) &= M_g(t_0) - [N_g(t_0)]^2 + [N_g(t)]^2 + \int_{t_0}^{t} dt' \Big\{ \Gamma_g(t,t') M_g(t') \\ &\quad + \Gamma_f(t') [2M_q(t') - M_g(t') + 2\{N_g(t') - N_q(t')\}^2] \Big\} \,. \end{aligned} \tag{6.72}$$

Downloaded from https://www.cambridge.org/core. UNIVERSIDAD AUTONOMA METROPOLITANA, on 15 Nov 2026 at 13:15:21, subject to the Cambridge Core terms of use, available at https://www.cambridge.org/core/terms. https://doi.org/10.1017/CBO9780511628788.007

Again retaining only the dominant term on the right-hand side, we see that $M_{q,g}$ should be asymptotically proportional to N_g^2. Substituting this form and using Eq. (6.71), we find

$$M_q \sim \left(1 + \frac{C_F}{3C_A}\right) N_q^2 , \quad M_g \sim \frac{4}{3} N_g^2 . \tag{6.73}$$

A quantity that is convenient experimentally is the relative size of the second multiplicity moment, measured by the ratio

$$R_{2,p} \equiv \frac{\langle n(n-1) \rangle_p}{\langle n \rangle_p^2} = \frac{M_p}{N_p^2} . \tag{6.74}$$

From Eqs. (6.68) and (6.73), we obtain the prediction

$$R_{2,e^+e^-} = \frac{M_q + N_q^2}{2N_q^2} \sim 1 + \frac{C_A}{6C_F} = \frac{11}{8} . \tag{6.75}$$

Eq. (6.75) implies that asymptotically the width of the multiplicity distribution should grow in proportion to its mean value, which is qualitatively in agreement with experiment. Similarly, the higher moments $\langle n^k \rangle$ are predicted to grow like $\langle n \rangle^k$. This means that the asymptotic multiplicity distribution can be represented by a scale-invariant function of $n/\langle n \rangle$,

$$P(n) \sim \frac{1}{\langle n \rangle} \Psi \left(\frac{n}{\langle n \rangle} \right) , \tag{6.76}$$

a property known as Koba-Nielsen-Olesen (KNO) scaling [20].

In quantitative terms, the asymptotic QCD prediction of the form of the KNO function Ψ is rather different from that observed experimentally. For example, the measured value of R_2 for charged particles in e^+e^- annihilation is about 1 instead of 11/8. The next-to-leading correction to Eq. (6.75) is in fact of order $\sqrt{\alpha_S}$ with a negative coefficient [21]

$$\begin{aligned} R_{2,e^+e^-} &\sim 1 + \frac{C_A}{6C_F} - \left[\frac{55}{108} \frac{C_A}{C_F} + \left(1 - 6\frac{C_F}{C_A}\right) \frac{n_f}{54C_A} \right] \sqrt{\frac{C_A \alpha_S}{2\pi}} \\ &= \frac{11}{8} (1 - 0.55\sqrt{\alpha_S}) . \end{aligned} \tag{6.77}$$

As shown in the lower plot of Fig. 6.2, the effect of the next-to-leading correction (6.77) is to bring the prediction for R_{2,e^+e^-} much closer to the measured value. The good agreement of the Lund (JETSET) prediction with the data suggests that hadronization and higher-order perturbative corrections can account for the remaining difference. The higher moments ratios R_k, defined by

$$R_k \equiv \langle n(n-1) \ldots (n-k+1) \rangle / \langle n \rangle^k , \tag{6.78}$$

Downloaded from https://www.cambridge.org/core. UNIVERSIDAD AUTONOMA METROPOLITANA, on 15 Nov 2026 at 13:15:21, subject to the Cambridge Core terms of use, available at https://www.cambridge.org/core/terms. https://doi.org/10.1017/CBO9780511628788.007

have similar corrections with coefficients that grow with k, making the next-to-leading-order predictions progressively less reliable for higher moments [21].

6.4 Quark and gluon jet differences

The results of the previous section suggest that there should be characteristic differences between jets initiated by quarks and gluons. For example, Eq. (6.71) predicts that the average multiplicity of *any* type of object in a gluon jet should become $C_A/C_F = 9/4$ times greater than that in a quark jet asymptotically, while Eq. (6.73) predicts that the asymptotic multiplicity distribution should also become wider for a gluon jet, by the square root of C_A/C_F.

These differences arise from the greater effective colour charge-squared of the gluon, which is proportional to C_A as opposed to C_F for the quark. The dominant asymptotic contribution to the multiplicity from a quark jet comes from the emission by the initial quark of a highly virtual gluon, which then generates a gluon jet. Thus one factor of C_A in the cascade is replaced by C_F, leading to a reduction in the average multiplicity by a factor of C_F/C_A. The second moment is reduced by the same factor, and so the width of the multiplicity distribution is also decreased.

As a consequence of the higher multiplicity, the fragmentation function of a gluon jet would be expected to be softer, *i.e.* more concentrated at low values of the momentum fraction x, than that of a quark jet. Actually, the treatment in Section 6.1.3 shows that the shape of the low-x fragmentation function – the Gaussian peak in $\ln(1/x)$ – is the same for quark and gluon jets in leading (and in fact also next-to-leading) logarithmic approximation. What *is* different is the height of the peak, which should again be in the ratio $C_F : C_A$ for quarks versus gluons asymptotically. To conserve momentum, this implies a relative reduction in the gluon fragmentation function at higher x.

Another characteristic difference is that gluon jets should be broader than quark jets. We saw in Section 3.3 that the Sterman-Weinberg two-jet fraction for e^+e^- annihilation takes the form (3.32) in lowest order, which means that the angular size δ_q of the quark jets for a given small energy fraction ϵ is

$$\delta_q \sim \exp\left[\frac{\pi(1-f_2)}{4C_F\alpha_S(s)\ln\epsilon}\right] . \tag{6.79}$$

Since $1/\alpha_S(s)$ increases logarithmically with energy, this means that the angular jet width, for a fixed Sterman-Weinberg fraction f_2, decreases like a negative power of s. For a final state consisting of two gluon jets, as

Downloaded from https://www.cambridge.org/core. UNIVERSIDAD AUTONOMA METROPOLITANA, on 15 Nov 2026 at 13:15:21, subject to the Cambridge Core terms of use, available at https://www.cambridge.org/core/terms. https://doi.org/10.1017/CBO9780511628788.007

would be seen in the decay of a $^1S_0$ heavy quark-antiquark bound state, for example, the analogous calculation gives a factor of C_A in place of C_F and therefore

$$\delta_g \sim \delta_q^{C_F/C_A} . \tag{6.80}$$

Thus the power decrease of the angular width is less rapid for gluon jets.

The experimental data on gluon jet properties show the predicted qualitative differences from quark jets, although at present energy scales the differences are less marked than those expected asymptotically [22,23]. For example, Fig. 6.10 shows the data of the OPAL collaboration on the fragmentation function for gluon jets produced in three-jet decays of Z^0 bosons into b quarks, $Z^0 \to b\bar{b}g$. The label '$k_\perp$ definition: $y_{\rm cut} = 0.02$' indicates that the k_T or Durham jet algorithm (3.33), with $y = 0.02$, was used to obtain the three-jet sample. The gluon jets were selected in the following way. The most energetic jet was assumed to be a quark jet, which is true in about 97% of events. Of the two remaining jets, one was 'tagged' as a b- or $\bar{b}$-quark jet by the presence of a secondary vertex due to the decay of a b-flavoured hadron. With about 93% probability, the remaining jet is then a gluon jet. The comparative points for light (uds) quark jets were obtained by a combination of anti-tagging secondary vertices and selecting jets that have a charged track with $x > 0.45$. In heavy-quark jets, this is less likely because of the weak decay of the heavy hadron. The data are corrected for the selection and detector effects; the correction factors are shown in the upper plot.

We see that the gluon fragmentation function is indeed softer than that for light quarks, with a higher peak at small x. A direct comparison with the b quark jets does not show such clear differences, because the b jets contain the products of the weak decay of the b-flavoured hadron, which also tend to be soft.

Notice that the gluon fragmentation function obtained from this analysis is consistent with that deduced from the longitudinal fragmentation function, Fig. 6.6.

6.5 Resummation of event shapes

As we discussed in Section 3.4, event shape variable distributions in e^+e^- annihilation provide some of the cleanest tests of QCD and a powerful way of determining the strong coupling α_S. The perturbative prediction of the thrust distribution, for example, has the form

$$\begin{aligned} \frac{1}{\sigma}\frac{d\sigma}{dT} &= \alpha_S(\mu^2)A_1(T) + [\alpha_S(\mu^2)]^2 A_2(T, s/\mu^2) \\ &\quad + [\alpha_S(\mu^2)]^3 A_3(T, s/\mu^2) + \cdots \end{aligned} \tag{6.81}$$

Downloaded from https://www.cambridge.org/core. UNIVERSIDAD AUTONOMA METROPOLITANA, on 15 Nov 2026 at 13:15:21, subject to the Cambridge Core terms of use, available at https://www.cambridge.org/core/terms. https://doi.org/10.1017/CBO9780511628788.007

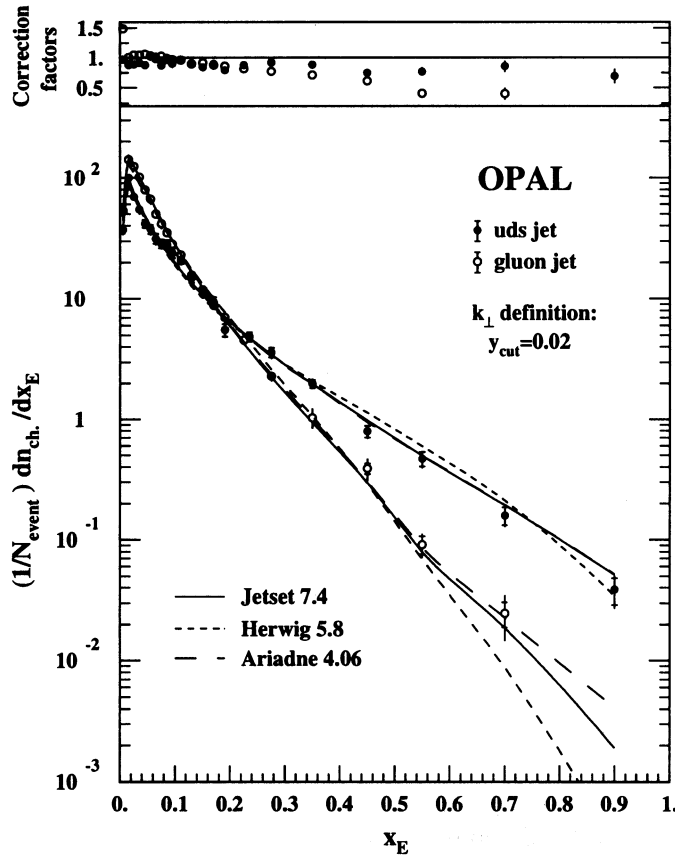


Fig. 6.10. Comparison between light (*uds*) quark and gluon jet fragmentation functions, and the predictions of various event generators. Figure from ref. [23].

where we know $A_1(T)$ and $A_2(T, s/\mu^2)$ in full. Thus a fit to the data neglecting the unknown higher-order terms yields a measured value of $\alpha_S(\mu^2)$. Assuming that A_3 is of order unity, we would expect a relative precision of the order of α_S^2 ($\sim 2\%$ at Z^0 energies).

In addition to the fact that we do not yet know the full form of A_3, a number of factors limit the reliability of the perturbative prediction.

1. *Large logarithms.* These enhance higher-order terms and limit the range of thrust that can be used for determining α_S. Near the two-jet configuration (*i.e.* at high thrust) the perturbative coefficients become very large:

$$A_n(T) \underset{T \to 1}{\sim} \frac{\ln^{2n-1}(1-T)}{1-T} . \tag{6.82}$$

Thus for the higher orders to be negligible it is not sufficient to have

Downloaded from https://www.cambridge.org/core. UNIVERSIDAD AUTONOMA METROPOLITANA, on 15 Nov 2026 at 13:15:21, subject to the Cambridge Core terms of use, available at https://www.cambridge.org/core/terms. https://doi.org/10.1017/CBO9780511628788.007

$\alpha_S \ll 1$; we need in fact $\alpha_S \ln^2(1-T) \ll 1$. This is a significant limitation, since most of the data are at high T, where $\alpha_S \ln^2(1-T) \sim 1$ even at the highest available energies.

2. *Renormalization scale dependence.* The coefficients beyond the first depend on the arbitrary renormalization scale μ^2 used in calculating them. For the second term we have explicitly

$$A_2(T, s/\mu^2) = A_2(T,1) - bA_1(T)\ln(s/\mu^2)\ , \tag{6.83}$$

where b is the first coefficient of the QCD β function, defined in Eq. (2.8). The scale dependence of A_2 is necessary in order to cancel that of the running coupling to the same order, see Eq. (3.21):

$$\alpha_S(\mu^2) = \alpha_S(s) + b\alpha_S^2 \ln(s/\mu^2) + \cdots\ , \tag{6.84}$$

but a residual scale dependence is left in order α_S^3. It is particularly worrying that the data are fitted best by using a small scale [24], $\mu^2 \ll s$, which generates large higher-order terms when expressed in terms of $\alpha_S(s)$. It might be argued that this corresponds to the fact that a physical scale much smaller than s, for example the typical transverse momentum of an emitted gluon $\mu^2 \sim (1-T)s$, is controlling the dynamics. However, physics should be independent of μ, which is just an artifact of our method of calculation. In any case, a change of scale cannot be the whole story, because this produces only one logarithmic factor for each power of α_S, whereas the coefficients (6.82) contain two such factors.

3. *Hadronization corrections.* As discussed in Section 5.6, hadronization is outside the domain of perturbation theory and its effects can only be estimated at present through the use of models, of which the most successful are those built into parton shower simulation programs [25,26]. In the programs, one can easily turn off the hadronization phase of the simulation and compare the distributions generated at the parton and hadron levels. However, modern shower simulations operate not by performing an exact perturbative calculation up to a fixed order, but rather by treating enhanced terms, such as the explicit logarithms described above, to all orders. They therefore generate parton configurations of arbitrarily high multiplicity, typically much larger than the maximum of four partons generated at order α_S^2, and are not well suited to estimating the hadronization corrections for fixed-order calculations.

The above difficulties can be alleviated by identifying the explicit large logarithms in each order of perturbation theory and resumming them to all orders. The resummation is most effective when the logarithmic terms

Downloaded from https://www.cambridge.org/core. UNIVERSIDAD AUTONOMA METROPOLITANA, on 15 Nov 2026 at 13:15:21, subject to the Cambridge Core terms of use, available at https://www.cambridge.org/core/terms. https://doi.org/10.1017/CBO9780511628788.007

exponentiate, *i.e.* when they combine in such a way that the logarithm of the cross section is less divergent in the two-jet limit. This is made more precise in the following subsection.

6.5.1 Exponentiation and resummation

Instead of working with the event shape distribution directly, it is convenient to introduce the event shape fraction, which for the thrust distribution is

$$f(\tau) = \int_{1-\tau}^{1} dT \, \frac{1}{\sigma} \frac{d\sigma}{dT} \, . \tag{6.85}$$

This quantity is somewhat analogous to the two-jet fraction f_2, with $\tau = 1 - T$ playing the role of the jet resolution y. By exponentiation of such a quantity, we mean more precisely that at small τ (high thrust)

$$f(\tau) = C(\alpha_S) \exp G[\alpha_S, \ln(1/\tau)] + D(\alpha_S, \tau) \tag{6.86}$$

where, writing the large logarithm as $L = \ln(1/\tau)$,

$$\begin{aligned} C(\alpha_S) &= 1 + \sum_{n=1}^{\infty} C_n a^n \, , \\ G(\alpha_S, L) &= \sum_{n=1}^{\infty} \sum_{m=1}^{n+1} G_{nm} a^n L^m \\ &\equiv L\, g_1(\alpha_S L) + g_2(\alpha_S L) + \alpha_S \, g_3(\alpha_S L) + \cdots \, , \end{aligned} \tag{6.87}$$

and the remainder $D(\alpha_S, \tau)$ vanishes as $\tau \to 0$. For later convenience we have defined $a = \alpha_S/2\pi$ in the expansions, and have suppressed the dependence on the renormalization scale μ^2 for the moment. The function g_1 resums all the *leading logarithms* $\alpha_S^n L^{n+1}$, while g_2 contains the *next-to-leading logarithmic* (NLL) terms $\alpha_S^n L^n$, and g_3 etc. represent the remaining *subdominant* logarithmic corrections $\alpha_S^n L^m$ with $0 < m < n$. The important point is that, whereas the event fraction itself has up to two factors of L for each power of α_S, its logarithm has only one extra L for each α_S. The double logarithms come purely from the expansion of the exponential function.

If exponentiation takes place and we know the leading and next-to-leading functions $g_1(u)$ and $g_2(u)$ of Eq. (6.87) in the region $u \lesssim 1$, then, provided the subdominant contributions $g_3(u)$ etc. behave reasonably in this region, we can predict $\ln f$ reliably for $\alpha_S L \lesssim 1$. This is a much larger region than the one $\alpha_S L^2 \ll 1$ in which the original perturbative expansion was applicable.

A knowledge of both $g_1(u)$ and $g_2(u)$ is necessary not only to extend the region of validity consistently to $\alpha_S L \lesssim 1$ but also to gain some control of

Downloaded from https://www.cambridge.org/core. UNIVERSIDAD AUTONOMA METROPOLITANA, on 15 Nov 2026 at 13:15:21, subject to the Cambridge Core terms of use, available at https://www.cambridge.org/core/terms. https://doi.org/10.1017/CBO9780511628788.007

the renormalization scale dependence of the prediction. This is because the scale dependence of the leading function $g_1(u)$ has to be cancelled order-by-order by contributions from $g_2(u)$. Thus $g_2(u)$ has a dependence on the renormalization scale μ^2, of the form

$$g_2(u,\mu^2) = g_2(u,s) - bu^2 \frac{dg_1}{du} \ln\left(\frac{s}{\mu^2}\right) , \tag{6.88}$$

which is the analogue of Eq. (6.83) for exponentiated quantities. As in the case of a fixed-order prediction, if the resulting resummed expression still shows a strong residual scale dependence, this can be taken as a warning that neglected higher-order terms may be anomalously large, since they have to cancel this dependence. Furthermore, since α_S itself is not defined until the scale is specified, the calculation of $g_2(u)$ is essential if one wishes to use resummation to improve the determination of α_S.

The exponentiation of event shapes follows primarily from the corresponding property of QCD matrix elements in the soft and collinear regions [27]. In addition, however, one must establish that the phase space defining the event fraction for a particular shape variable does not spoil this property near the two-jet limit. Schematically we have

$$f(\tau) = \frac{1}{\sigma} \sum_n \int |\mathcal{M}_n|^2 d\Phi_n(\tau) \tag{6.89}$$

where $\Phi_n(\tau)$ defines the n-parton phase space for shape values bounded by τ. One has to show essentially that each term in the sum factorizes at small τ, possibly after some suitable integral transformation of Eq. (6.89), in such a way that successive terms form an exponential series. The coherent branching formalism developed in the previous chapter is very useful for this purpose [28]. Usually the problem can be recast in the form of an integral equation, whose solution gives the exponent function $G(\alpha_S, L)$ directly. It should be emphasized that the exponentiation of the event fraction has only been established for a limited number of event shape variables, and for some variables it is known that exponentiation does *not* occur.

In the case of the thrust and some related event shapes, exponentiation may be established through a connection with the jet mass distribution. Each event can be divided into two jet hemispheres by the plane orthogonal to the thrust axis. Suppose that the invariant masses-squared of the multiparticle systems in the two hemispheres are k^2 and $\bar{k}^2$. Then since the thrust is simply proportional to the resultant three-momentum in each hemisphere, it is related to k^2 and $\bar{k}^2$ by elementary two-body kinematics. At high thrust we have explicitly

$$T = 1 - k^2/s - \bar{k}^2/s - 2k^2\bar{k}^2/s^2 + \dots \ . \tag{6.90}$$

Downloaded from https://www.cambridge.org/core. UNIVERSIDAD AUTONOMA METROPOLITANA, on 15 Nov 2026 at 13:15:21, subject to the Cambridge Core terms of use, available at https://www.cambridge.org/core/terms. https://doi.org/10.1017/CBO9780511628788.007

The last term shown is of order τ^2 and so it and higher terms contribute only to the remainder function $D(\alpha_S, \tau)$ in Eq. (6.86). Hence to logarithmic accuracy we can write schematically

$$\Phi_n(\tau) = \Phi_n(k^2 + \bar{k}^2 < s) \, . \tag{6.91}$$

Thus to the required accuracy the event fraction can be written in terms of $J(\bar{k}^2, s)$, the jet mass distribution measured at scale s, as

$$f(\tau) = \int_0^{\tau s} dk^2 \int_0^{\tau s - k^2} d\bar{k}^2 J(k^2, s) J(\bar{k}^2, s) \, . \tag{6.92}$$

This expression can be factorized in terms of the Laplace transform

$$\tilde{J}_\nu(s) = \int_0^\infty dk^2 e^{-\nu k^2} J(k^2, s) \, . \tag{6.93}$$

One finds that

$$f(\tau) = \frac{1}{2\pi i} \int_C \frac{d\nu}{\nu} e^{\nu \tau s} [\tilde{J}_\nu(s)]^2 \tag{6.94}$$

where the inverse transform contour C lies to the right of all singularities of the integrand. A derivation of the Laplace-transformed jet mass distribution $\tilde{J}_\nu(s)$ to NLL accuracy may be found in ref. [29].

In this way one finds that the function $g_1(u = \alpha_S L)$ which resums the leading logarithms is [30,31]

$$g_1(u) = -\frac{C_F}{\pi b^2 u} \left[(1 - 2bu) \ln(1 - 2bu) - 2(1 - bu) \ln(1 - bu) \right] \, . \tag{6.95}$$

At small u, $g_1(u) \sim -C_F u / \pi$, giving

$$f(\tau) \sim \exp(-2aC_F L^2) \tag{6.96}$$

in the limit $\alpha_S L \ll 1$. We see that the dominant effect of resummation is to suppress the event fraction at small τ, leading to a turn-over instead of a divergence in the distribution at high thrust. This is a Sudakov form factor effect: in order for an event to have very high thrust, the produced quark and antiquark must have emitted very little gluon bremsstrahlung, which is very improbable. Note however that the double logarithmic approximation (6.96) is not reliable in the vicinity of the turn-over, since it predicts that the latter occurs at $\alpha_S L = \pi / 2C_F = 1.2$, which is inconsistent with the assumption that $\alpha_S L \ll 1$. Using the full leading-logarithmic result (6.95) gives a turn-over at lower thrust, $\alpha_S L \sim 0.5$.

The next-to-leading function g_2 is found to be [28]

$$g_2(u) = \; - \; \frac{C_F \kappa}{2\pi^2 b^2} \Big[2 \ln(1 - bu) - \ln(1 - 2bu) \Big]$$

Downloaded from https://www.cambridge.org/core. UNIVERSIDAD AUTONOMA METROPOLITANA, on 15 Nov 2026 at 13:15:21, subject to the Cambridge Core terms of use, available at https://www.cambridge.org/core/terms. https://doi.org/10.1017/CBO9780511628788.007

$$
\begin{aligned}
&- \frac{3C_F}{2\pi b}\ln(1-bu) - \frac{2\gamma_E C_F}{\pi b}\Big[\ln(1-bu) - \ln(1-2bu)\Big] \\
&- \frac{C_F b'}{\pi b^2}\Big[\ln(1-2bu) - 2\ln(1-bu) \\
&+ \tfrac{1}{2}\ln^2(1-2bu) - \ln^2(1-bu)\Big] \\
&- \ln\Gamma(1 - g_1(u) - u g_1'(u)) \,, \qquad (6.97)
\end{aligned}
$$

where $\kappa = (201 - 9\pi^2 - 10n_f)/18$, $\gamma_E = 0.5772\ldots$ is the Euler constant, and b' is the second β function coefficient defined in Eq. (2.8). If we renormalize at a scale $\mu^2 \neq s$, g_2 receives an extra contribution as specified in Eq. (6.88).

The same approach yields a very similar formula [32] for the distribution of the 'heavy jet mass' $\rho = \mathrm{Max}\{k^2, \bar{k}^2\}/s$. Other quantities that have been fully resummed to NLL accuracy after being shown to exponentiate include the energy-energy correlation [33] and an shape variable called the 'jet broadening', which measures the transverse energy relative to the thrust axis [34].

6.5.2 *Combining with fixed-order predictions*

To obtain an improved prediction throughout the whole of phase space we should combine the resummed expression, valid at small τ, with the full second-order result, valid elsewhere. This is equivalent to evaluating the remainder function $D(\alpha_S, \tau)$ in Eq. (6.86).

The simplest procedure is the so-called 'log matching' scheme, in which one recasts Eq. (6.86) in the form

$$\ln f(\tau) = K(\alpha_S) + G(\alpha_S, L) + H(\alpha_S, \tau) \qquad (6.98)$$

where again $K(\alpha_S)$ represents a power series in α_S and $H(\alpha_S, \tau)$ is a remainder that vanishes as $\tau \to 0$. Writing the full second-order prediction as

$$f(\tau) = 1 + aA(\tau) + a^2 B(\tau) + O(\alpha_S^3) \,, \qquad (6.99)$$

we have

$$\ln f(\tau) = aA(\tau) + a^2\{B(\tau) - \tfrac{1}{2}[A(\tau)]^2\} + O(\alpha_S^3) \,. \qquad (6.100)$$

The functions $A(\tau)$ and $B(\tau)$ are conveniently tabulated in ref. [35].

To resum logarithmic terms of order α_S^3 and beyond, we should add $G(\alpha_S, L)$ to this expression after subtracting its first- and second-order parts, which are already included in $A(\tau)$ and $B(\tau)$. Hence the resummed prediction with $K(\alpha_S)$ and $H(\alpha_S, \tau)$ evaluated to second order is

$$
\begin{aligned}
\ln f(\tau) \;&=\; Lg_1(\alpha_S L) + g_2(\alpha_S L) + a(A(\tau) - G_{11}L - G_{12}L^2) \\
&+\; a^2(B(\tau) - \tfrac{1}{2}[A(\tau)]^2 - G_{22}L^2 - G_{23}L^3) \,, \qquad (6.101)
\end{aligned}
$$

Downloaded from https://www.cambridge.org/core. UNIVERSIDAD AUTONOMA METROPOLITANA, on 15 Nov 2026 at 13:15:21, subject to the Cambridge Core terms of use, available at https://www.cambridge.org/core/terms. https://doi.org/10.1017/CBO9780511628788.007

where the functions g_1 and g_2 are given in Eqs. (6.95) and (6.97) respectively, and the coefficients G_{nm} are obtained by expanding them to second order:

$$\begin{aligned} G_{11} &= +3C_F \\ G_{12} &= -2C_F \\ G_{22} &= -\tfrac{4}{3}\pi^2 C_F^2 + \left(\tfrac{1}{3}\pi^2 - \tfrac{169}{36}\right) C_F C_A + \tfrac{11}{18} C_F n_f \\ G_{23} &= -\tfrac{11}{3} C_F C_A + \tfrac{2}{3} C_F n_f \ . \end{aligned} \qquad (6.102)$$

Notice that in this matching scheme the subdominant term $a^2 G_{21} L$, representing the first contribution from $\alpha_S g_3(\alpha_S L)$ in Eq. (6.87), is implicitly included and exponentiated as a part of $B(\tau)$. Thus the largest missing subdominant contribution is of order $\alpha_S^3 L^2$, which is suppressed by four large logarithms relative to the leading term in $f(\tau)$ of this order. Other matching procedures can be defined, which differ by subdominant terms of the same order and thus are equally valid, but in general they require more care to ensure the exponentiation of subdominant logarithms [28].

The resummation and matching procedure described above yields the results shown in Fig. 6.11. The effects of resummation become large for $T > 0.9$. At lower thrust the effect is still appreciable but can be compensated by a change of renormalization scale. In fact, the resummed curve is fortuitously reproduced quite well by the fixed-order formula if one uses a very low scale ($\mu^2 \sim 0.001 s$), combined with a smaller value of $\alpha_S(M_Z^2)$. This explains the empirical preference for low scales remarked on earlier.

Several experimental studies have been performed comparing resummed event shape predictions with data [36-40]. An example is shown in Fig. 6.12. We see that after hadronization corrections the prediction compares well with the data over a wide range of thrust, although the corrections become large and rapidly-varying outside the fitted region. The label $f = 1$ indicates the scale choice $\mu^2 = s$. The error shown for α_S is the statistical error of the fitting procedure only. The total experimental error of ± 0.002 is small compared to the theoretical uncertainties coming from scale dependence and hadronization, estimated at around ± 0.005.

The results of resummed determinations of α_S will be summarized in Chapter 12. The most important general feature of these analyses is that they no longer show a preference for small values of the renormalization scale μ^2: indeed a fit usually cannot be obtained for $\mu^2 \ll s$. Since the principal large logarithms have been explicitly resummed, there is no dynamical argument for using a scale much different from s, and most resummed analyses quote a theoretical uncertainty corresponding to a rather small range of scales around $\mu^2 \sim s$. This, combined with a somewhat reduced scale dependence in the region $\mu^2 \sim s$, leads to a reduction

Downloaded from https://www.cambridge.org/core. UNIVERSIDAD AUTONOMA METROPOLITANA, on 15 Nov 2026 at 13:15:21, subject to the Cambridge Core terms of use, available at https://www.cambridge.org/core/terms. https://doi.org/10.1017/CBO9780511628788.007

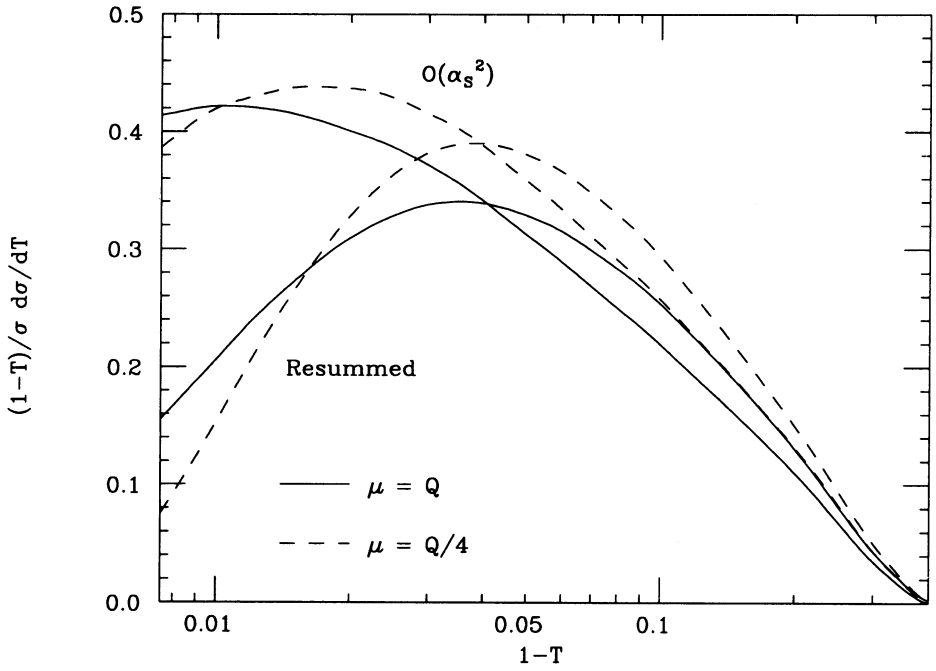


Fig. 6.11. Fixed-order and resummed predictions for the thrust distribution in $Z^0 \to$ hadrons, for five-flavour $\Lambda_{\overline{\rm MS}} = 250$ MeV $[\alpha_S(M_Z^2) = 0.120]$, without hadronization corrections. Adapted from ref. [28].

in the quoted uncertainties in α_S due to scale dependence. The central values of α_S are slightly larger than those obtained from fixed-order analyses, since the small scales preferred by the latter tend to be correlated with smaller values of α_S.

6.6 Resummation of jet rates

The large logarithms that occur in the e^+e^- n-jet fractions f_n at small values of the jet resolution parameter y ($y_{\rm cut}$) can also be resummed using the coherent branching formalism [41], provided the jets are defined using the k_T (Durham) jet clustering algorithm described in Section 3.3. By comparing the definition Eq. (3.38) of the jet resolution with Eq. (5.97) for the coherent evolution variable (called t in this chapter), we see that in order for the two final-state jets from a branching to be resolvable we require that

$$\min[z^2, (1-z)^2]t > sy \,, \tag{6.103}$$

Downloaded from https://www.cambridge.org/core. UNIVERSIDAD AUTONOMA METROPOLITANA, on 15 Nov 2026 at 13:15:21, subject to the Cambridge Core terms of use, available at https://www.cambridge.org/core/terms. https://doi.org/10.1017/CBO9780511628788.007

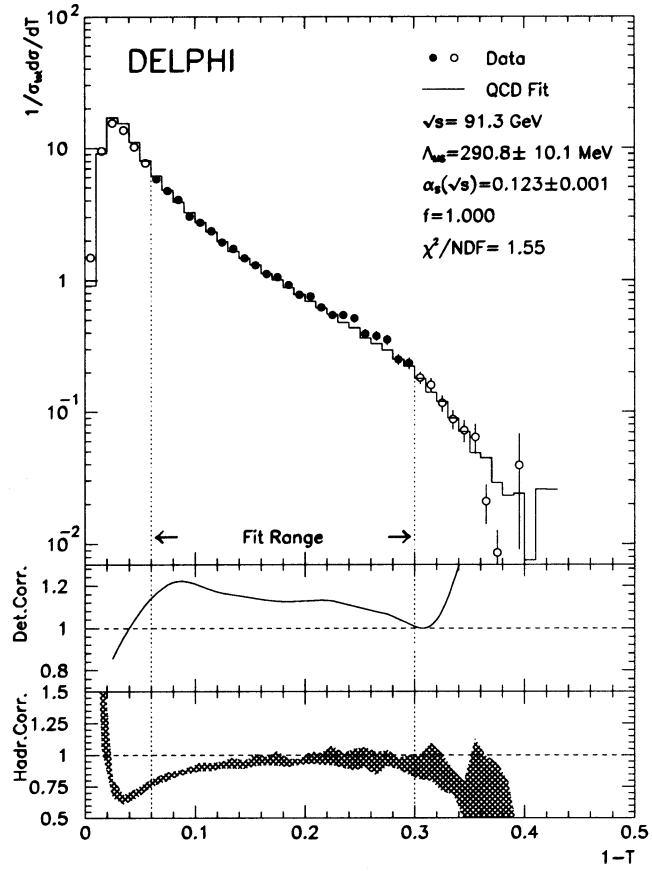


Fig. 6.12. Resummed prediction for the thrust distribution in $Z^0 \to$ hadrons, corrected for hadronization, fitted to data of the DELPHI collaboration. The lower curves show the detector and hadronization correction factors. Figure from ref. [39].

i.e. that

$$\sqrt{t_0/t} < z < 1 - \sqrt{t_0/t} \tag{6.104}$$

where

$$t_0 \equiv sy \; . \tag{6.105}$$

The boundary condition (6.104) is precisely equivalent to the infra-red cut-off condition (5.99), with the reinterpretation (6.105) of the cut-off in terms of the jet resolution. It means that exactly one jet can be resolved in a quark or gluon jet at scale $t = t_0$, and hence that

$$\phi_{q,g}(u, t_0) = u \tag{6.106}$$

Downloaded from https://www.cambridge.org/core. UNIVERSIDAD AUTONOMA METROPOLITANA, on 15 Nov 2026 at 13:15:21, subject to the Cambridge Core terms of use, available at https://www.cambridge.org/core/terms. https://doi.org/10.1017/CBO9780511628788.007

in the generating function formalism of Section 6.2.

Inserting the boundary values (6.106) in Eqs. (6.58) and (6.63), we obtain equations for the absolutely normalized jet generating functions in next-to-leading logarithmic approximation, which can be used to predict the jet rates at small values of y by repeated differentiation at $u = 0$. In terms of the Sudakov form factors (6.60,6.64), defining

$$\Delta_f(t) = [\Delta_q(t)]^2/\Delta_g(t) \,, \tag{6.107}$$

one finds

$$\begin{aligned} f_2(s,y) &= [\Delta_q(s)]^2 \,, \\ f_3(s,y) &= 2\,[\Delta_q(s)]^2 \int_{t_0}^{s} dt\, \Gamma_q(s,t)\Delta_g(t) \,, \\ f_4(s,y) &= 2\,[\Delta_q(s)]^2 \left\{ \left[\int_{t_0}^{s} dt\, \Gamma_q(s,t)\Delta_g(t) \right]^2 \right. \\ &+ \int_{t_0}^{s} dt\, \Gamma_q(s,t)\Delta_g(t) \int_{t_0}^{t} dt' \left[\Gamma_g(t,t')\Delta_g(t') \right. \\ &+ \left. \left. \Gamma_f(t')\Delta_f(t') \right] \right\} . \end{aligned} \tag{6.108}$$

We see that a simple exponentiation of $\ln y$ terms is valid for the two-jet fraction f_2, whereas the higher multijet rates satisfy a form of exponentiation only in the pseudo-Abelian limit $\Gamma_g, \Gamma_f \to 0$:

$$f_{k+2}(s,y) = \frac{1}{k!} \left[2 \int_{t_0}^{s} dt\, \Gamma_q(s,t) \right]^k \cdot [\Delta_q(s)]^2 + (\Gamma_g \text{ and } \Gamma_f \text{ terms}) \,. \tag{6.109}$$

Data on the y (y_{cut}) dependence of the jet fractions at LEP are shown in Fig. 6.13. The curves are from the JETSET event generator, which includes the above physics in its parton shower simulation, together with a string hadronization model, as discussed in Section 5.7. All the multijet fractions have the same qualitative behaviour: they rise rapidly with decreasing y reach a maximum and then fall off again at very small y. The fall-off comes from the Sudakov form factor, which appears as an overall factor expressing the fact that it becomes increasingly difficult to keep the jet multiplicity fixed as the k_T resolution becomes very fine. Notice that the effect of hadronization, shown by the difference between the dashed and solid curves, is to increase the number of jets resolved at the smallest values of y.

Downloaded from https://www.cambridge.org/core. UNIVERSIDAD AUTONOMA METROPOLITANA, on 15 Nov 2026 at 13:15:21, subject to the Cambridge Core terms of use, available at https://www.cambridge.org/core/terms. https://doi.org/10.1017/CBO9780511628788.007

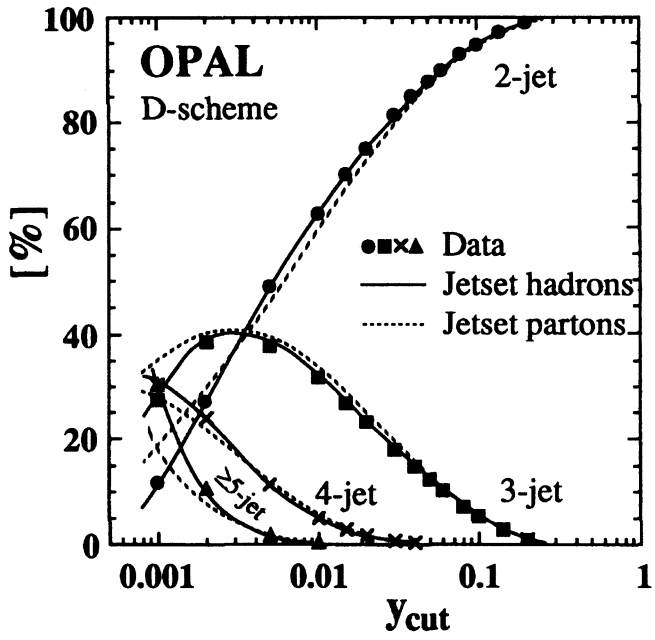


Fig. 6.13. OPAL data and JETSET predictions for multijet rates in e^+e^- annihilation at 91 GeV. Figure from ref. [42].

6.7 Average jet multiplicity

A study of the mean multiplicity of jets rather than hadrons in e^+e^- annihilation offers many experimental and theoretical advantages [43]. On the experimental side, the dependence of this quantity on jet resolution tests the same kind of physics as the energy dependence and can be studied in a single experiment at fixed energy. Furthermore, every hadronic event contributes at every value of the resolution, so the statistical and systematic errors are greatly reduced.

From the theoretical viewpoint, the jet multiplicity has the advantage of being fully computable in perturbation theory. There is no arbitrary normalization parameter, and the specified k_T-resolution scale $t_0 = s\,y$ ($y \equiv y_{\rm cut}$) takes the place of the infra-red cut-off parameter in the hadron multiplicity calculation. At large values of y the jet multiplicity is reliably predicted by fixed-order perturbation theory, while at small values, for the k_T algorithm, large logarithms can be resummed using the generating function formalism. Finally at very small y, where t_0 is of the order of the hadronization scale, we can hope to learn about the hadronization process

Downloaded from https://www.cambridge.org/core. UNIVERSIDAD AUTONOMA METROPOLITANA, on 15 Nov 2026 at 13:15:21, subject to the Cambridge Core terms of use, available at https://www.cambridge.org/core/terms. https://doi.org/10.1017/CBO9780511628788.007

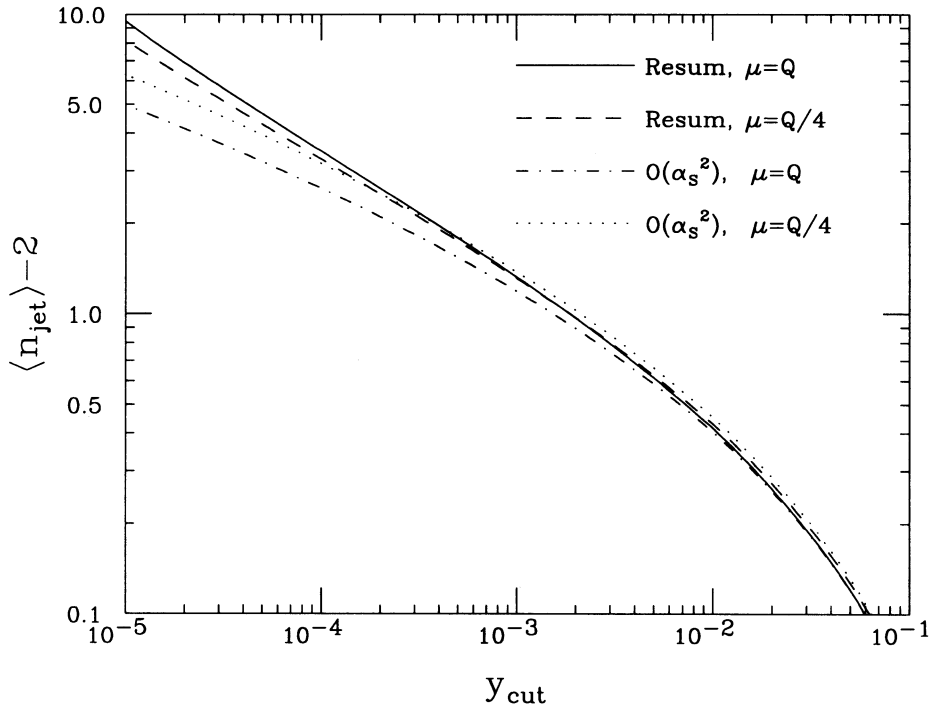


Fig. 6.14. Fixed-order and resummed predictions for the mean jet multiplicity in $Z^0 \to$ hadrons, for $\Lambda_{\overline{\rm MS}} = 250$ MeV, without hadronization corrections.

by comparing the extrapolated perturbative prediction with experimental data.

To any fixed order α_S^n, the mean jet multiplicity $\langle n_{\rm jet} \rangle$ is given by the multijet fractions computed to the same order. The $O(\alpha_S^2)$ predictions at $s = M_Z^2$ for different values of the renormalization scale μ^2 are shown in Fig. 6.14. The dependence on the renormalization scale is seen to be fairly weak, making the mean jet multiplicity a good quantity for the determination of α_S.

Like the multijet rates, the mean jet multiplicity contains double logarithms that dominate at small values of y. But whereas in the exclusive rates these logarithms sum up mainly to provide a universal Sudakov suppression, in the inclusive multiplicity they generate a rapidly rising behaviour, with a rate of increase greater than any power of $L = \ln(1/y)$. Keeping only the double-logarithmic terms, one finds explicitly that

$$\begin{aligned} \langle n_{\rm jet} \rangle &= 2 + aC_F L^2 + \tfrac{1}{12} a^2 C_F C_A L^4 + \tfrac{1}{360} a^3 C_F C_A^2 L^6 + \ldots \\ &= 2 + 2\frac{C_F}{C_A}(\cosh\sqrt{aC_A L^2} - 1) \end{aligned} \tag{6.110}$$

Downloaded from https://www.cambridge.org/core. UNIVERSIDAD AUTONOMA METROPOLITANA, on 15 Nov 2026 at 13:15:21, subject to the Cambridge Core terms of use, available at https://www.cambridge.org/core/terms. https://doi.org/10.1017/CBO9780511628788.007

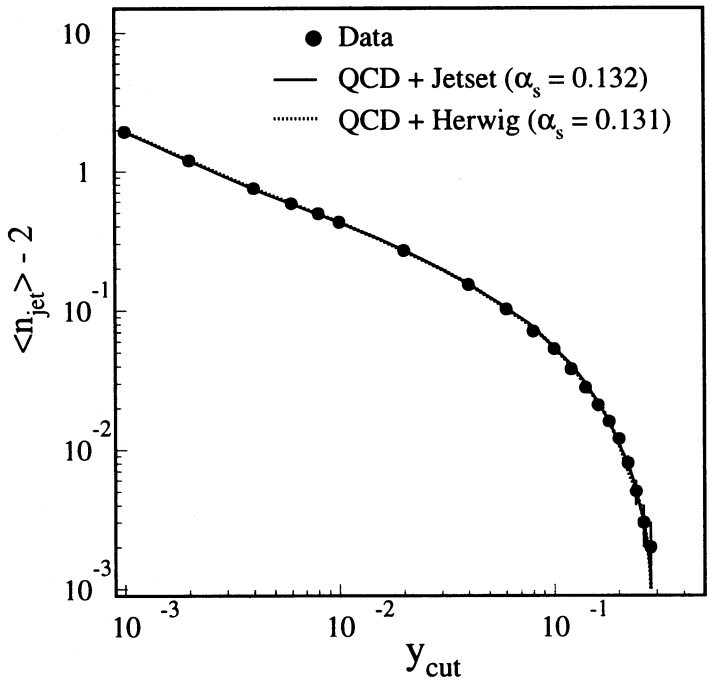


Fig. 6.15. Resummed prediction for the mean jet multiplicity in $Z^0 \to$ hadrons, corrected for hadronization, fitted to data of the L3 collaboration. Figure from ref. [37].

$$\sim \frac{C_F}{C_A} \exp \sqrt{aC_A L^2} \, .$$

This is the analogue of the $\exp \sqrt{\ln s}$ behaviour of the hadron multiplicity, Eq. (6.37). In fact, recalling that $a = \alpha_S(s)/2\pi = 1/2\pi b \ln(s/\Lambda)$ and $y = t_0/s$, we have

$$\sqrt{aC_A L^2} \simeq \sqrt{\frac{2C_A}{\pi b}} \left[\sqrt{\ln\left(\frac{s}{\Lambda^2}\right)} - \sqrt{\ln\left(\frac{t_0}{\Lambda^2}\right)} \right] , \qquad (6.111)$$

as long as $\alpha_S L \ll 1$ (even if $\alpha_S L^2 \gg 1$).

Notice that in the double-logarithmic approximation the nth order term in Eq. (6.110) has colour factor $C_F C_A^{n-1}$. This means that the dominant contribution comes from emission of a single gluon from the quark or antiquark, followed by multiple branching within the gluon jet. We also see how an asymptotic dependence on $\sqrt{\alpha_S}$ is obtained from a power series in α_S when one drops the exponentially decreasing part of the sum.

The prediction can again be extended to next-to-leading logarithmic accuracy by means of the coherent branching formalism. The jet multi-

Downloaded from https://www.cambridge.org/core. UNIVERSIDAD AUTONOMA METROPOLITANA, on 15 Nov 2026 at 13:15:21, subject to the Cambridge Core terms of use, available at https://www.cambridge.org/core/terms. https://doi.org/10.1017/CBO9780511628788.007

plicities satisfy the coupled integral equations (6.69) with the inhomogeneous terms $N_{q,g}(t_0) = 1$. Solutions to these equations can be obtained in closed form in terms of modified Bessel functions [9,43].

As in the case of event shape distributions, the NLL prediction can be improved further by matching with the exact two-loop result, after subtraction of the logarithmic terms that have been resummed. The resulting prediction for e^+e^- annihilation is shown in Fig. 6.14.

We should note that, since $\langle n_{\rm jet} \rangle$ does not have the simple exponentiating form (6.86), the resummation of leading $(\alpha_S^n L^{2n})$ and next-to-leading $(\alpha_S^n L^{2n-1})$ logarithms does not fully include the renormalization scale dependence of even the leading terms, which is of order $\alpha_S^{n+1} L^{2n} = \alpha_S^{n+1} L^{2(n+1)-2}$, *i.e.* next-to-next-to-leading. Therefore the determination of α_S from jet multiplicity is only strictly reliable at larger y. As illustrated in Fig. 6.15, the prediction is in very good agreement with experiment for a value of $\alpha_S(M_Z^2)$ consistent with that found from event shape analyses.

Although we have considered here the mean jet multiplicity in e^+e^- annihilation, similar arguments can be applied to other hard processes, such as deep inelastic scattering (DIS) [44]. In such cases we also have to deal with 'initial-state' jets, *i.e.* those associated with incoming coloured partons. The multiplicity of initial-state jets depends not only on the momentum transfer-squared of the hard process (Q^2 in DIS) but also on the momentum fraction carried by the incoming struck parton (Bjorken x in DIS). If the struck parton has high x, it is less likely to have emitted initial-state jets, and so the jet multiplicity is reduced. Conversely an incoming parton at small x is more likely to have emitted jets, and so the multiplicity is enhanced at small x. The momentum not carried by emitted jets is carried by the 'beam jet(s)', which consists of unresolvable collinear and/or soft initial-state emission, together with the remnant partons of the incoming hadron(s) and any further hadrons produced in soft interactions of the remnants.

References

1) J.C. Collins and D.E. Soper, *Ann. Rev. Nucl. Part. Sci.* **37** (1987) 383.

2) G. Curci, W. Furmanski and R. Petronzio, *Nucl. Phys.* **B175** (1980) 27; E.G. Floratos, C. Kounnas and R. Lacaze, *Nucl. Phys.* **B192** (1981) 417.

3) W. Furmanski and R. Petronzio, preprint TH.2933–CERN (1980); *Phys. Lett.* **B97** (1980) 437.

4) P. Nason and B.R. Webber, *Nucl. Phys.* **B421** (1994) 473.

5) ALEPH collaboration, D. Buskulic *et al.*, *Phys. Lett.* **B357** (1995) 487; *ibid.* **B364** (1995) 247 (erratum).

6) I.I. Balitsky and V.M. Braun, *Nucl. Phys.* **B361** (1991) 93.

Downloaded from https://www.cambridge.org/core. UNIVERSIDAD AUTONOMA METROPOLITANA, on 15 Nov 2026 at 13:15:21, subject to the Cambridge Core terms of use, available at https://www.cambridge.org/core/terms. https://doi.org/10.1017/CBO9780511628788.007

7) A.H. Mueller, *Nucl. Phys.* **B213** (1983) 85; erratum quoted in *ibid.* **B241** (1984) 141; *ibid.* **B228** (1983) 351.

8) M. Schmelling, *Physica Scripta* **51** (1995) 683.

9) Yu.L. Dokshitzer, V.A. Khoze, A.H. Mueller and S.I. Troyan, *Basics of Perturbative QCD*, Editions Frontières, Paris (1991).

10) C.P. Fong and B.R. Webber, *Nucl. Phys.* **B355** (1992) 54.

11) TASSO collaboration, W. Braunschweig *et al.*, *Zeit. Phys.* **C47** (1990) 187.

12) OPAL collaboration, D. Akrawy *et al.*, *Phys. Lett.* **B247** (1990) 617.

13) L3 collaboration, B. Adeva *et al.*, *Phys. Lett.* **B259** (1991) 199.

14) OPAL collaboration, R. Akers *et al.*, *Zeit. Phys.* **C68** (1995) 203.

15) G. Altarelli, R.K. Ellis, G. Martinelli and S-Y. Pi, *Nucl. Phys.* **B160** (1979) 301.

16) P.J. Rijken and W.L. van Neerven, Leiden preprint INLO-PUB-4/96.

17) R.P. Feynman, *Photon Hadron Interactions*, W.A. Benjamin, New York (1972).

18) Yu.L. Dokshitzer, V.A. Khoze and S.I. Troyan, in *Perturbative Quantum Chromodynamics*, ed. A.H. Mueller, World Scientific, Singapore (1989).

19) ZEUS collaboration, M. Derrick *et al.*, *Zeit. Phys.* **C67** (1995) 93.

20) Z. Koba, H.B. Nielsen and P. Olesen, *Nucl. Phys.* **B40** (1972) 317.

21) E.D. Malaza and B.R. Webber, *Nucl. Phys.* **B267** (1986) 702.

22) TASSO collaboration, W. Braunschweig *et al.*, *Zeit. Phys.* **C45** (1989) 1;
AMY collaboration, Y.K. Kim *et al.*, *Phys. Rev. Lett.* **63** (1989) 1772;
OPAL collaboration, G. Alexander *et al.*, *Phys. Lett.* **B265** (1991) 462; P.D. Acton *et al.*, *Zeit. Phys.* **C58** (1993) 387; R. Akers *et al.*, *Zeit. Phys.* **C68** (1995) 179.

23) OPAL collaboration, G. Alexander *et al.*, *Zeit. Phys.* **C69** (1996) 543.

24) ALEPH collaboration, D. Decamp *et al.*, *Phys. Lett.* **B234** (1990) 399; *ibid.* **B255** (1991) 623; *ibid.* **B257** (1991) 479;
DELPHI collaboration, P. Aarnio *et al.*, *Phys. Lett.* **B240** (1990) 271; *ibid.* **B247** (1990) 167;
L3 collaboration, B. Adeva *et al.*, *Phys. Lett.* **B237** (1990) 136; *ibid.* **B248** (1990) 464;
OPAL collaboration, M.Z. Akrawy *et al.*, *Phys. Lett.* **B252** (1990) 159, *Zeit. Phys.* **C47** (1990) 505; *ibid.* **C49** (1991) 375.

25) T. Sjöstrand, *Comp. Phys. Comm.* **39** (1984) 347;
M. Bengtsson and T. Sjöstrand, *Comp. Phys. Comm.* **43** (1987) 367.

26) G. Marchesini and B.R. Webber, *Nucl. Phys.* **B310** (1988) 461;
G. Marchesini, B.R. Webber, G. Abbiendi, I.G. Knowles, M.H. Seymour and L. Stanco, *Comp. Phys. Comm.* **67** (1992) 465.

27) Yu.L. Dokshitzer, and D.I. Dyakonov, *Phys. Lett.* **B84** (1979) 234;
G. Parisi and R. Petronzio, *Nucl. Phys.* **B154** (1979) 427;
A. Bassetto, M. Ciafaloni and G. Marchesini, *Nucl. Phys.* **B163** (1980) 477;
G. Curci and M. Greco, *Phys. Lett.* **B92** (1980) 175;
J.C. Collins and D.E. Soper, *Ann. Rev. Nucl. Part. Sci.* **37** (1987) 383.

28) S. Catani, L. Trentadue, G. Turnock and B.R. Webber, *Nucl. Phys.* **B407** (1993) 3.

29) S. Catani and L. Trentadue, *Phys. Lett.* **B217** (1989) 539, *Nucl. Phys.* **B327** (1989) 353; *ibid.* **B353** (1991) 183.

30) M. Greco, *Phys. Rev.* **D23** (1981) 2791.

31) K. Tesima and M.F. Wade, *Zeit. Phys.* **C52** (1991) 43.

32) S. Catani, G. Turnock and B.R. Webber, *Phys. Lett.* **B272** (1991) 368.

33) J. Kodaira and L. Trentadue, *Phys. Lett.* **B123** (1982) 335;
J.C. Collins and D.E. Soper, *Nucl. Phys.* **B284** (1987) 253;
G. Turnock, Cambridge preprint Cavendish–HEP–91/3, unpublished.

34) S. Catani, G. Turnock and B.R. Webber, *Phys. Lett.* **B295** (1992) 269.

Downloaded from https://www.cambridge.org/core. UNIVERSIDAD AUTONOMA METROPOLITANA, on 15 Nov 2026 at 13:15:21, subject to the Cambridge Core terms of use, available at https://www.cambridge.org/core/terms. https://doi.org/10.1017/CBO9780511628788.007

35) Z. Kunszt, P. Nason, G. Marchesini and B.R. Webber, in *Z Physics at LEP 1*, CERN Yellow Book 89-08, vol. 1, p. 373 (1989).

36) ALEPH collaboration, D. Decamp *et al.*, *Phys. Lett.* **B284** (1992) 163.

37) L3 collaboration, O. Adriani *et al.*, *Phys. Lett.* **B284** (1992) 471.

38) OPAL collaboration, P.D. Acton *et al.*, *Zeit. Phys.* **C59** (1993) 1.

39) DELPHI collaboration, P. Abreu *et al.*, *Zeit. Phys.* **C59** (1993) 21.

40) SLD collaboration, K. Abe *et al.*, *Phys. Rev.* **D51** (1995) 962.

41) S. Catani, Yu.L. Dokshitzer, M. Olsson, G. Turnock and B.R. Webber, *Phys. Lett.* **B269** (1991) 432.

42) OPAL collaboration, P.D. Acton *et al.*, *Zeit. Phys.* **C55** (1992) 1.

43) S. Catani, Yu.L. Dokshitzer, F. Fiorani and B.R. Webber, *Nucl. Phys.* **B377** (1992) 445.

44) S. Catani, Yu.L. Dokshitzer and B.R. Webber, *Phys. Lett.* **B322** (1994) 263.

Downloaded from https://www.cambridge.org/core. UNIVERSIDAD AUTONOMA METROPOLITANA, on 15 Nov 2026 at 13:15:21, subject to the Cambridge Core terms of use, available at https://www.cambridge.org/core/terms. https://doi.org/10.1017/CBO9780511628788.007